Article

Organometallic Uranium(V)#Imido Halide Complexes: From Synthesis to Electronic Structure and Bonding

Christopher R. Graves, Ping Yang, Stosh A. Kozimor, Anthony E. Vaughn, David L. Clark, Steven D. Conradson, Eric J. Schelter, Brian L. Scott, J. D. Thompson, P. Jeffrey Hay, David E. Morris, and Jaqueline L. Kiplinger

J. Am. Chem. Soc., **2008**, 130 (15), 5272-5285 • DOI: 10.1021/ja711010h • Publication Date (Web): 26 March 2008

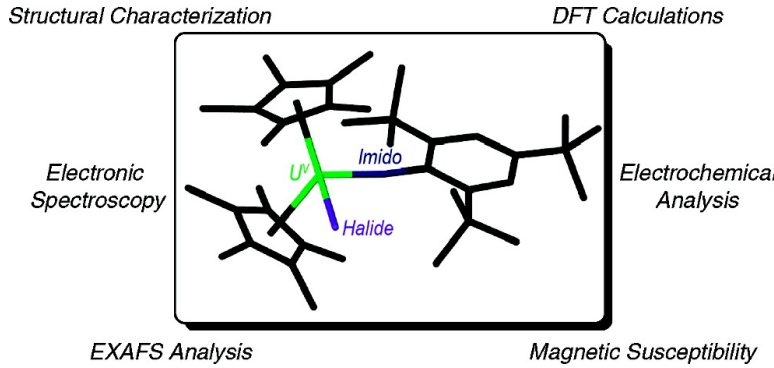

More About This Article

Additional resources and features associated with this article are available within the HTML version:

- Supporting Information
- Links to the 9 articles that cite this article, as of the time of this article download
- Access to high resolution figures
- Links to articles and content related to this article
- Copyright permission to reproduce figures and/or text from this article

View the Full Text HTML

J|A|C|S
ARTICLES

Published on Web 03/26/2008

Organometallic Uranium(V)−Imido Halide Complexes: From Synthesis to Electronic Structure and Bonding

Christopher R. Graves, Ping Yang, Stosh A. Kozimor, Anthony E. Vaughn, David L. Clark, Steven D. Conradson, Eric J. Schelter, Brian L. Scott, J. D. Thompson, P. Jeffrey Hay,* David E. Morris,* and Jaqueline L. Kiplinger*

Los Alamos National Laboratory, Los Alamos, New Mexico 87545

Received December 11, 2007; E-mail: kiplinger@lanl.gov

Abstract: Reaction of $(C_5Me_5)_2U(=N\text{-}2,4,6\text{-}{}^tBu_3\text{-}C_6H_2)$ or $(C_5Me_5)_2U(=N\text{-}2,6\text{-}{}^iPr_2\text{-}C_6H_3)(THF)$ with 5 equiv of CuX_n ($n = 1$, X = Cl, Br, I; $n = 2$, X = F) affords the corresponding uranium(V)−imido halide complexes, $(C_5Me_5)_2U(=N\text{-}Ar)(X)$ (where Ar = 2,4,6-${}^tBu_3$-C_6H_2 and X = F (**3**), Cl (**4**), Br (**5**), I (**6**); Ar = 2,6-${}^iPr_2$-C_6H_3 and X = F (**7**), Cl (**8**), Br (**9**), I (**10**)), in good isolated yields of 75–89%. These compounds have been characterized by a combination of single-crystal X-ray diffraction, ^{1}H NMR spectroscopy, elemental analysis, mass spectrometry, cyclic voltammetry, UV–visible−NIR absorption spectroscopy, and variable-temperature magnetic susceptibility. The uranium L_{III}-edge X-ray absorption spectrum of $(C_5Me_5)_2U(=N\text{-}2,4,6\text{-}{}^tBu_3\text{-}C_6H_2)(Cl)$ (**4**) was analyzed to obtain structural information, and the $U{=}N_{imido}$ (1.97(1) Å), U−Cl (2.60(2) Å), and $U-C_5Me_5$ (2.84(1) Å) distances were consistent with those observed for compounds **3**, **5**, **6**, **8**–**10**, which were all characterized by single-crystal X-ray diffraction studies. All $(C_5Me_5)_2U(=N\text{-}Ar)(X)$ complexes exhibit U^V/U^{IV} and U^{VI}/U^V redox couples by voltammetry, with the potential separation between these metal-based couples remaining essentially constant at ∼1.50 V. The electronic spectra are comprised of $\pi\rightarrow\pi^*$ and $\pi\rightarrow nb_{5f}$ transitions involving electrons in the metal−imido bond, and metal-centered f−f bands illustrative of spin–orbit and crystal-field influences on the $5f^1$ valence electron configuration. Two distinct sets of bands are attributed to transitions derived from this $5f^1$ configuration, and the intensities in these bands increase dramatically over those found in spectra of classical $5f^1$ actinide coordination complexes. Temperature-dependent magnetic susceptibilities are reported for all complexes with μ_{eff} values ranging from 2.22 to 2.53 μ_B. The onset of quenching of orbital angular momentum by ligand fields is observed to occur at ∼40 K in all cases. Density functional theory results for the model complexes $(C_5Me_5)_2U(=N\text{-}C_6H_5)(F)$ (**11**) and $(C_5Me_5)_2U(=N\text{-}C_6H_5)(I)$ (**12**) show good agreement with experimental structural and electrochemical data and provide a basis for assignment of spectroscopic bands. The bonding analysis describes multiple bonding between the uranium metal center and imido nitrogen which is comprised of one σ and two π interactions with variable participation of 5f and 6d orbitals from the uranium center.

Introduction

The complexes of the light actinide elements present an important challenge toward the understanding of electronic structure, bonding, and reactivity, as they often deviate from the chemical principles established for either the transition metals or the lanthanides, and while bonding in f-element complexes has generally been considered to be ionic, the issue of covalency remains an important subject of debate.[1–3] Recent work in our group has focused on the organometallic chemistry of both thorium and uranium,[4–9] with the goal of understanding unprecedented structures and reaction pathways, to develop a broad knowledge base for the elucidation of the aforementioned fundamental questions in actinide chemistry. The role that oxidation state plays in bonding is also of great interest in these studies. Compared to the more common tetravalent and hexavalent organouranium complexes,[10,11] pentavalent systems are rare, presumably as a consequence of their instability. Indeed, most of our current knowledge regarding the structures, electrochemical behavior, spectroscopic properties, and magnetic susceptibil-

(1) Diaconescu, P. L.; Arnold, P. L.; Baker, T. A.; Mindiola, D. J.; Cummins, C. C. *J. Am. Chem. Soc.* **2000**, *122*, 6108–6109.
(2) Mazzanti, M.; Wietzke, R.; Pecaut, J.; Latour, J.-M.; Maldivi, P.; Remy, M. *Inorg. Chem.* **2002**, *41*, 2389–2399.
(3) Meyer, K.; Mindiola, D. J.; Baker, T. A.; Davis, W. M.; Cummins, C. C. *Angew. Chem., Int. Ed.* **2000**, *39*, 3063–3066.
(4) Schelter, E. J.; Morris, D. E.; Scott, B. L.; Kiplinger, J. L. *Chem. Commun.* **2007**, 1029–1031.
(5) Schelter, E. J.; Yang, P.; Scott, B. L.; Da Re, R. E.; Jantunen, K. C.; Martin, R. L.; Hay, P. J.; Morris, D. E.; Kiplinger, J. L. *J. Am. Chem. Soc.* **2007**, *129*, 5139–5152.
(6) Pool, J. A.; Scott, B. L.; Kiplinger, J. L. *Chem. Commun.* **2005**, 2591–2593.
(7) Pool, J. A.; Scott, B. L.; Kiplinger, J. L. *J. Alloys Compd.* **2006**, *418*, 178–183.
(8) Kiplinger, J. L.; Scott, B. L.; Schelter, E. J.; Pool Davis Tournear, J. A. *J. Alloys Compd.* **2007**, *444–445*, 477–482.
(9) Schelter, E. J.; Yang, P.; Scott, B. L.; Thompson, J. D.; Martin, R. L.; Hay, P. J.; Morris, D. E.; Kiplinger, J. L. *Inorg. Chem.* **2007**, *46*, 7477–7488.
(10) Burns, C. J.; Eisen, M. S. Organoactinide Chemistry: Synthesis and Characterization. In *The Chemistry of the Actinide and Transactinide Elements*, 3rd ed.; Morss, L. R., Edelstein, N. M., Fuger, J., Eds.; Springer: The Netherlands, 2006; Vol. 5, pp 2799–2910 and references therein.
(11) Ephritikhine, M. *Dalton Trans.* **2006**, 2501–2516.

10.1021/ja711010h CCC: $40.75

ity for this oxidation state comes from classical coordination complexes of the halides, (e.g., UX_5, where X = halide).[12–15] While pentavalent uranium complexes containing metal–nitrogen and metal–oxygen bonds have been reported in recent years,[16,17] very few examples of organometallic uranium(V) complexes have been documented and thoroughly characterized,[18,19] and the development of a general synthetic strategy for the preparation of stable pentavalent organouranium complexes is desirable.

Our recent explorations into electrochemical trends of uranium organometallic complexes[20] revealed a surprisingly accessible, chemically reversible one-electron metal-based U^V/U^{IV} redox couple for $(C_5Me_5)_2U(=N\text{-}2,4,6\text{-}{}^tBu_3\text{-}C_6H_2)$ (**1**)[21] ($E_{1/2}$ = –0.73 V vs $[(C_5H_5)_2Fe]^{+/0}$), demonstrating that the electrochemically generated U^V species of **1** is stable on the voltammetric time scale. Analogous behavior is observed for the sterically less-congested $(C_5Me_5)_2U(=N\text{-}2,6\text{-}{}^iPr_2\text{-}C_6H_3)$ (THF) (**2**)[19,22] ($E_{1/2}$ = –0.86 V vs $[(C_5H_5)_2Fe]^{+/0}$).[23] These voltammetric observations suggested that isolable organometallic U^V−imido complexes are viable, provided a suitable chemical oxidant can be identified. We recently communicated a simple synthetic procedure for the one-electron oxidation of the U^{IV}−imido complexes **1** and **2** with copper(I) salts to give the corresponding U^V−imido(X) complexes (X = I, SPh, OTf) in good isolated yield.[23] This reaction pathway has allowed for the systematic study of a series of pentavalent uranium complexes. The in-depth synthetic protocol, as well as the crystallographic, electrochemical, spectroscopic, and magnetic characterization of the U^V−imido halide series (halide = F, Cl, Br, I), paired with a computational study to investigate the electronic structure of this new class of uranium complexes, is presented herein.

Results and Discussion

Synthesis and Structural Characterization. Equations 1 and 2 display the synthetic protocol utilized and yields obtained in the preparation of the U^V−imido halides. Treatment of a toluene solution of either **1** (eq 1) or **2** (eq 2) with excess Cu−halide oxidant[24] at room temperature generates the corresponding U^V−imido halide complexes **3**–**10** as dark brown solids in 75–89% isolated yields. Following workup by filtration through Celite and crystallization, all complexes were reproducibly isolated as analytically pure solids and were characterized by a combination of ^1H NMR, electrochemistry, UV–visible−NIR spectroscopy, elemental and mass spectrometric analyses, magnetic susceptibility, and X-ray crystallography.[25]

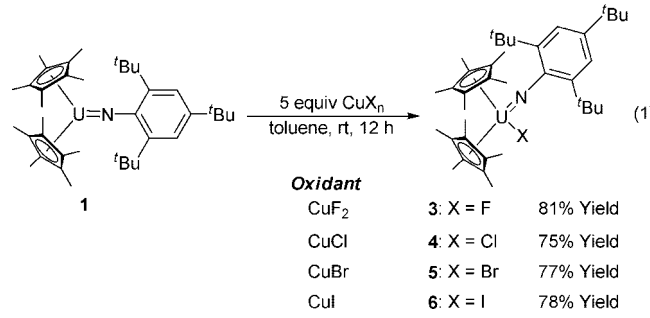

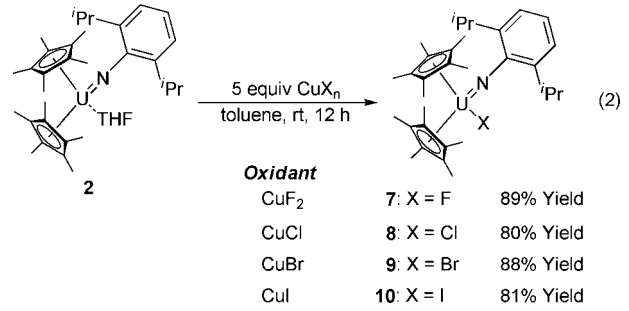

Although silver(I) salts are routine oxidants for organometallic complexes and have been utilized in the chemical oxidation of uranium compounds,[26,27] reports of analogous Cu(I) oxidations are quite rare, with only a few examples in the literature limited to the oxidation of electron-rich transition metal species.[28,29] Furthermore, as Ag(I)-promoted oxidations are often difficult to predict and control,[27] the use of inexpensive, readily available,

(12) Bagnall, K. W. In *Comprehensive Coordination Chemistry*; Wilkinson, G., Gillard, R. D., Mc Cleverty, J. A., Eds.; Pergamon: Oxford, 1987; Vol. 3, p 1129.
(13) For a review on the synthesis, stability, and properties of pentavalent uranium, see: Selbin, J.; Ortego, J. D. *Chem. Rev.* **1969**, *69*, 657–621.
(14) For recent advances in the chemistry of pentavalent uranyl complexes, see: (a) Natrajan, L.; Burdet, F.; Pecaut, J.; Mazzanti, M. *J. Am. Chem. Soc.* **2006**, *128*, 7152–7153. (b) Burdet, F.; Pecaut, J.; Mazzanti, M. *J. Am. Chem. Soc.* **2006**, *128*, 16512–16513. (c) Berthet, J.-C.; Siffredi, G.; Thuery, P.; Ephritikhine, M. *Chem. Commun.* **2006**, 3184–3186. (d) Arnold, P. L.; Patel, D.; Wilson, C.; Love, J. B. *Nature* **2008**, *451*, 315–318.
(15) Ryan, J. L. *J. Inorg. Nucl. Chem.* **1971**, *33*, 153–177.
(16) For representative examples of U^V amide and alkoxide stabilized complexes, see: (a) Zalkin, A.; Brennan, J. G.; Andersen, R. A. *Acta Crystallogr.* **1988**, *C44*, 1553–1554. (b) Roussel, P.; Hitchcock, P. B.; Tinker, N. D.; Scott, P. *Inorg. Chem.* **1997**, *36*, 5716–5721. (c) Castro-Rodriguez, I.; Olsen, K.; Meyer, K. *Inorg. Chem.* **2003**, *125*, 4564–4571. (d) Salmon, P.; Thuery, P.; Ephritikhine, M. *Polyhedron* **2007**, *26*, 631–636.
(17) Castro-Rodriguez, I.; Olsen, K.; Gantzel, P.; Meyer, K. *J. Am. Chem. Soc.* **2003**, *125*, 4565–4571.
(18) For examples of pentavalent organouranium complexes, see: (a) Boisson, C.; Berthet, J.-C.; Lance, M.; Nierlich, M.; Vigner, J.; Ephritikhine, M. *J. Chem. Soc., Chem. Commun.* **1995**, 543–544. (b) Gourier, D.; Caurant, D. *Inorg. Chem.* **1997**, *36*, 5931–5936. (c) Ephritikhine, M.; Berthet, J. C.; Boisson, C.; Lance, M.; Nierlich, M. *J. Alloys Compd.* **1998**, *271−273*, 144–149. (d) Boaretto, R.; Roussel, P.; Alcock, N. W.; Kingsley, A. J.; Munslow, I. J.; Sanders, C. J.; Scott, P. *J. Organomet. Chem.* **1999**, *591*, 174–184. (e) Arliguie, T.; Rourmigue, M.; Ephritikhine, M. *Organometallics* **2000**, *19*, 109–111.
(19) Arney, D. S. J.; Burns, C. J. *J. Am. Chem. Soc.* **1993**, *115*, 9840–9841.
(20) Morris, D. E.; Da Re, R. E.; Jantunen, K. C.; Castro-Rodriguez, I.; Kiplinger, J. L. *Organometallics* **2004**, *23*, 5142–5153.
(21) Arney, D. S. J.; Burns, C. J. *J. Am. Chem. Soc.* **1995**, *117*, 9448–9460.
(22) Herein, we also report the structural characterization of complex **2**, with crystalline product being obtained from the slow evaporation of a concentrated pentanes solution at room temperature, yielding 86% of the recovered product. See the Supporting Information for a thermal ellipsoid representation and crystallographic experimental parameters, as well as a table of bond lengths and angles.
(23) Graves, C. R.; Scott, B. L.; Morris, D. E.; Kiplinger, J. L. *J. Am. Chem. Soc.* **2007**, *129*, 11914–11915.
(24) While CuCl, CuBr, and CuI are all readily available from commercial sources, CuF is not. The present oxidation protocol is also applicable to the use of CuX_2 as the one-electron oxidant, and CuF_2, which is available, acted as the appropriate oxidant in the synthesis of both **3** and **7**.
(25) For the characterization data for **3**−**5** and **7**−**9**, see the Supporting Information. For the characterization data for **6** and **10**, see ref 23.
(26) For examples of the oxidation of uranium complexes utilizing Ag(I) salts as the oxidant, see: (a) Burns, C. J.; Smith, W. H.; Huffman, J. C.; Sattelberger, A. P. *J. Am. Chem. Soc.* **1990**, *112*, 3237–3239. (b) Boisson, C.; Berthet, J.-C.; Lance, M.; Nierlich, M.; Viger, J.; Ephritikhine, M. *J. Chem. Soc., Chem. Commun.* **1995**, 543–544. (c) Maynadié, J.; Berthet, J.-C.; Thuery, P.; Ephritikhine, M. *Organometallics* **2007**, *26*, 4585–4591.
(27) Connelly, N. G.; Geiger, W. E. *Chem. Rev.* **1996**, *96*, 877–910.

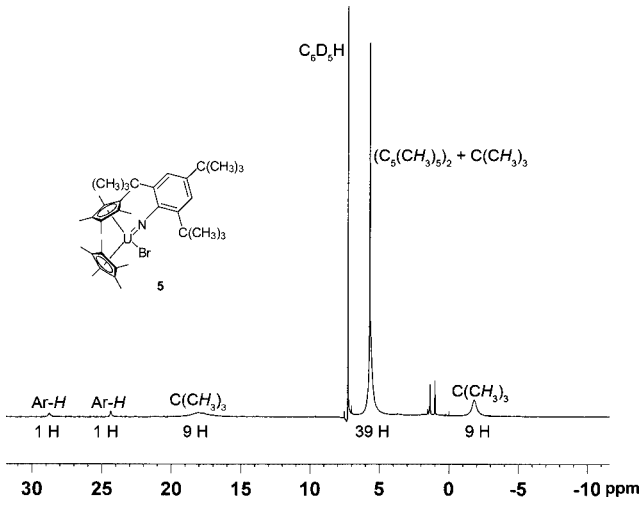

Figure 1. ^{1}H NMR spectrum of $(C_5Me_5)_2U(=N\text{-}2,4,6\text{-}^tBu_3\text{-}C_6H_2)(Br)$ (**5**).

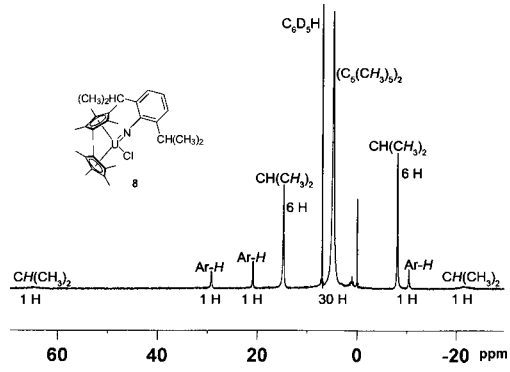

Figure 2. ^{1}H NMR spectrum of $(C_5Me_5)_2U(=N\text{-}2,6\text{-}^iPr_2\text{-}C_6H_3)(Cl)$ (**8**).

and diverse Cu(I) salts as oxidants provides a versatile and useful synthetic advancement.

These paramagnetic uranium(V) complexes were characterized by ^{1}H NMR spectroscopy. Complexes **3**–**6** exhibit a broad[30] signal at ~4–6 ppm, corresponding to the $C_5\mathit{Me}_5$ ligand protons. Further, there is an inequivalency of the *ortho* ^{t}Bu groups, which is not observed in the U^{IV}−imido starting material.[21] Similar ^{1}H NMR spectra were observed for the U^V−^{i}Pr−imido halides **7**–**10**: a broad signal at ~4–6 ppm, corresponding to the $C_5\mathit{Me}_5$ ligand protons and inequivalent ^{i}Pr groups. Representative ^{1}H NMR spectra for the U^V−^{t}Bu−imido halides and the U^V−^{i}Pr−imido halides are shown in Figures 1 and 2, respectively.

Interestingly, there is a relationship between the chemical shift for analogous protons (i.e., the $C_5\mathit{Me}_5$ resonances) and the identity of halogen atom in the paramagnetic $(C_5Me_5)_2U(=N\text{-}2,6\text{-}^iPr_2\text{-}C_6H_3)(X)$ structure, with the chemical shift of the $C_5\mathit{Me}_5$ group moving upfield with variation of the halogen from I → Br → Cl → F.[31] Similar trends have been observed for other paramagnetic trivalent and tetravalent uranium systems,[32] and while the exact reasons for this phenomenon have been widely discussed and contested,[33–35] in the uranium systems it has been proposed that the trend results from variation in the amount of π donation from the halogen atom to the metal center across the series.[32a,c] In effect, the better the π donor (F > Cl > Br > I), the more electron-rich the uranium center, manifesting in a larger shielding of the auxiliary protons and an upfield shift of the resonances for those protons. This reasoning is in accord with electrochemical findings, which suggest that the fluoride derivatives **3** and **7** are more electron-rich at the metal center than their Cl/Br/I counterparts (*vide infra*).

X-ray diffraction studies confirmed the identity of the U^V−imido halides. Representative structures are provided for complexes **3** and **8** in Figure 3, and selected geometric parameters for complexes **3**, **5**, **6**, **8**–**10** are presented in Table 1. Single crystals could not be obtained for **4** and **7**, but their formulations are consistent with ^{1}H NMR, mass spectrometry, and elemental analysis, as well as electrochemical, spectroscopic, and magnetic characterization data. The crystallographic parameters for **3**, **5**, **6**, **8**–**10** are provided in the Supporting Information.

The molecular structures for both the ^{t}Bu and ^{i}Pr U^V−imido halide series feature a typical bent-metallocene framework with the imido and halide ligands contained within the metallocene wedge, similar in constitution to the related $(C_5Me_5)_2U(=O)(O\text{-}2,6\text{-}^iPr_2\text{-}C_6H_3)$ U^V−oxo alkoxide complex.[19] All of the U^V−imido halide complexes have nearly linear $U{=}N{-}C_{Ar}$ angles (169.6(4)−172.2(9)°) and short $U{=}N_{imido}$ bond distances (1.958(6)−1.975(6) Å), with no obvious trends present on the basis of donating ability of the halide. These metrical parameters compare well with those reported for other high-valent uranium (U^{IV}−U^{VI})−imido compounds. The U^V−imido structures $(C_5H_4Me)_3U(=N\text{-}C_6H_5)$[36] and $[(Me_3Si)_2N]_3U(=N\text{-}4\text{-}Me\text{-}C_6H_4)$[37] have $U{=}N_{imido}$ bond distances of 2.019(6) and 1.940(6) Å and $U{=}N{-}C_{Ar}$ angles of 167.4(6)° and 171.4(5)°, respectively. U^{VI}−imido complexes show similar geometric parameters: $(C_5Me_5)_2U(=N\text{-}C_6H_5)_2$[38] has $U{=}N_{imido}$ bond distance of 1.952(7) Å and $U{=}N{-}C_{Ar}$ angle of 177.8(6)°, while $(C_5Me_5)_2U(=N\text{-}$

(28) Leigh, J. S.; Whitmire, K. H.; Yee, K. A.; Albright, T. A. *J. Am. Chem. Soc.* **1989**, *111*, 2726–2727.
(29) Rabier, A.; Lugan, N.; Mathieu, R.; Geoffroy, G. L. *Organometallics* **1994**, *13*, 4676–4678.
(30) For example, complexes **6** and **10** have $\Delta\nu_{1/2}$ values of 93 and 125 Hz, respectively.
(31) The chemical shifts for the ($C_5\mathit{Me}_5$) protons in the ^{1}H NMR spectrum for **7**−**10** are as follows: δ 3.94 ppm (**7**, X = F), 4.92 ppm (**8**, X = Cl), 5.31 ppm (**9**, X = Br), and 5.78 ppm (**10**, X = I).
(32) This trend in chemical shift for like protons as a function of halide has been seen for other paramagnetic uranium systems. (a) $[(1,3\text{-}R_2C_5H_3)_2UX]_2$ (R = $SiMe_3$, CMe_3; X = F, Cl, Br, I): Lukens, W. W., Jr.; Beshouri, S. M.; Stuart, A. L.; Andersen, R. A. *Organometallics* **1999**, *18*, 1247–1252. (b) $(C_5Me_5)_3UX$ (X = F, Cl, Br): Evans, W. J.; Nyce, G. W.; Johnston, M. A.; Ziller, J. W. *J. Am. Chem. Soc.* **2000**, *122*, 12019–12020. (c) $(1,3\text{-}R_2C_5H_3)_2UX_2$ (R = $SiMe_3$, CMe_3; X = F, Cl, Br, I): Lukens, W. W., Jr.; Beshouri, S. M.; Blosch, L. L.; Stuart, A. L.; Andersen, R. A. *Organometallics* **1999**, *18*, 1235–1246. The ^{1}H NMR behavior of the $(C_5H_5)_3U$−X system has also been extensively studied, (Fisher, R. D. NMR-Spectroscopy of organo-f-element and pre-lanthanoid complexes. In *Fundamental and Technological Aspects of Organo-f-Element Chemistry*; Marks, T. J., Fragala, I. L., Eds.; NATO ASI Series C: Mathematical and Physical Sciences; D. Reidel Publishing Co.: Dordrecht, 1985; Vol. 155, p 294), not only for X = halide but also for other donor groups, such as OR, NR_2, SR, PR_2, etc.
(33) Dhingra, M. M.; Ganguli, P.; Mitra, S. *Chem. Phys. Lett.* **1974**, *25*, 579–581.
(34) Drago, R. S.; Wayland, B. B. *Inorg. Chem.* **1968**, *7*, 628–630.
(35) LaMar, G. N.; Fischer, R. H.; Horrocks, W. D., Jr. *Inorg. Chem.* **1967**, *6*, 1798–1803.
(36) Brennan, J. G.; Andersen, R. A. *J. Am. Chem. Soc.* **1985**, *107*, 514–516.
(37) Stewart, J. L. Tris[bis(trimethylsilyl)amido]uranium: Compounds with Tri-, Tetra-, and Pentavalent Uranium. Ph.D. Dissertation, Univeristy of California, Berkeley, CA, 1988.
(38) Arney, D. S. J.; Burns, C. J.; Smith, D. C. *J. Am. Chem. Soc.* **1992**, *114*, 10068–10069.

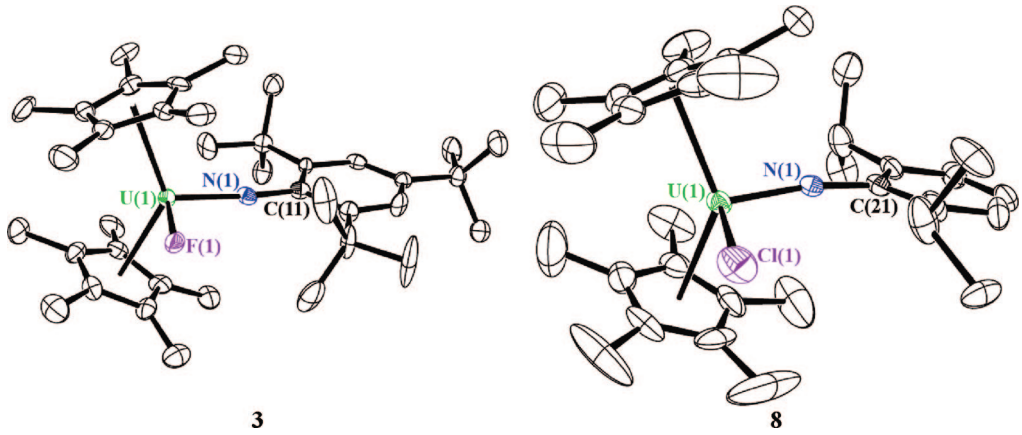

Figure 3. Molecular structures of complexes **3** and **8**, with thermal ellipsoids projected at the 50% probability level. Hydrogen atoms have been omitted for clarity.

Table 1. Selected Metrical Parameters for Complexes **3**, **5**, **6**, and **8–10**

	3 (X = F)	**5** (X = Br)	**6** (X = I)	**8** (X = Cl)	**9** (X = Br)	**10** (X = I)
U−X (Å)	2.122(5)	2.7744(10)	3.0116(6)	2.6209(15)	2.789(3)	3.0385(7)
U=N (Å)	1.965(8)	1.958(6)	1.975(6)	1.963(4)	1.969(7)	1.974(7)
N−C_{Ar} (Å)	1.415(11)	1.424(9)	1.418(8)	1.404(7)	1.40(2)	1.406(10)
N−U−X (°)	97.0(3)	96.11(18)	97.20(16)	105.79(13)	105.3(2)	106.6(2)
U=N−C_{Ar} (°)	171.0(7)	169.8(5)	169.7(5)	169.6(4)	172.2(9)	170.7(6)

2,6-^{i}Pr$_2$-C$_6$H$_3$)(=O)[19] has corresponding values of 1.988(4) Å and 170.5(4)°. These geometric parameters demonstrate that U=N bond distances and U=N−C angles in uranium−imido complexes are insensitive to oxidation state. In fact, the U=N_{imido} distances and U=N−C_{Ar} angles for the U^{IV}−imido starting materials (**1**,[21] 1.952(12) Å, 162.3(10)°; **2**,[22] 2.006(5) Å, 172.6(5)°) also fall within the same range as for the U^{V}−imido halides reported in the present work.

As expected on the basis of the ionic radius of the halogen atoms,[39] the U−X bond length increases down the series, with U−F < U−Cl < U−Br < U−I.[40] At 2.122(5) Å, the U−F bond distance observed in **3** compares well with those for other known pentavalent uranium fluoride complexes[41] and falls within range of distances reported for other high-valent uranium compounds that have been structurally characterized containing a U−F bond. Uranium(V) complexes containing a U−Cl bond have been previously structurally characterized, with typical bond lengths ranging from 2.4 to 2.7 Å.[4243,44] At 2.6209(15) Å, the U−Cl bond length observed for **8** fits in this range and also compares well with metrical parameters observed for other organometallic uranium complexes exhibiting U−Cl bonds.[45] Several pentavalent uranium complexes are also known containing a U−Br bond, with distances ranging between 2.6 and 2.9 Å,[46,47] a range that includes those distances found for both **5** (2.7744(10) Å) and **9** (2.789(3) Å). To the best of our knowledge, there are no structurally characterized pentavalent iodide complexes; however, the distances reported for **6** (3.0116(6) Å) and **10** (3.0385(7) Å) fall in the range of other structurally reported U−I distances.[48,49]

EXAFS Analysis of (C_5Me_5)$_2$U(=N-2,4,6-^{t}Bu$_3$-C$_6$H$_2$)(Cl). While (C_5Me_5)$_2$U(=N-2,4,6-^{t}Bu$_3$-C$_6$H$_2$)(Cl) (**4**) was isolated in high yield (75%) in a crystalline form, the crystals were not suitable for analysis by single-crystal X-ray experiments.

(39) Cotton, F. A.; Wilkinson, G.; Bochmann, M.; Murillo, C. *Advanced Inorganic Chemistry*, 6th ed.; John Wiley & Sons, Inc.: New York, 1998; p 548.

(40) For a detailed list of various U^{V} halide complexes, see: Grenthe I.; Drozdzynski, J.; Fujino, T.; Buck, E. C.; Albrecht-Schmitt, T. E.; Wolf, S. F. Uranium. In *The Chemistry of the Actinide and Transactinide Elements*, 3rd ed.; Morss, L. R., Edelstein, N. M., Fuger, J., Eds.; Springer: The Netherlands, 2006; Vol. 1, pp 501–529.

(41) α- and β-UF_5 have U−F bond distances in the range of 2.18–2.30 Å (Zachariasen, W. H. *Acta Crystallogr.* **1949**, *2*, 296–298), while (2,2′-bipyridyl)UF_5 has U−F bond lengths of 2.04–2.06 Å (Arnaudet, L.; Bougon, R.; Ban, B.; Lance, M.; Nierlich, M.; Vigner, J. *Inorg. Chem.* **1994**, *33*, 4510–4516). For detailed crystallographic parameters for a series of anionic [X][UF_6] complexes, see:(a) Brown, D. *The Halides of the Lanthanides and Actinides*; Wiley Interscience: New York, 1968. (b) Penneman, R. A.; Ryan, R. R.; Rosenzweig, A. *Struct. Bonding (Berlin)* **1973**, *13*, 1–52.

(42) U−F distances in the range of ∼2.1–2.4 Å have been reported for tetra- and hexavalent uranium complexes. For examples, see: (a) Ryan, R. R.; Penneman, R. A.; Kanellakopulos, B. *J. Am. Chem. Soc.* **1975**, *97*, 4258–4260. (b) Burns, C. J.; Smith, W. H.; Huffman, J. C.; Sattelberger, A. P. *J. Am. Chem. Soc.* **1990**, *112*, 3237–3239. (c) Lukens, W. W., Jr.; Beshouri, S. M.; Blosch, L. L.; Stuart, A. L.; Andersen, R. A. *Organometallics* **1999**, *18*, 1235–1246. (d) Evans, W. J.; Nyce, G. W.; Johnston, M. A.; Ziller, J. W. *J. Am. Chem. Soc.* **2000**, *122*, 12019–21020.

(43) Smith, G. S.; Johnson, Q.; Elson, R. E. *Acta Crystallogr.* **1967**, *22*, 300–303.

(44) Wedler, M.; Noltemeyer, M.; Edelmann, F. T. *Angew. Chem., Int. Ed.* **1992**, *31*, 72–75.

(45) For representative examples of U−Cl distances for other uranium oxidation states, see: (a) Zalkin, A.; Beshouri, S. M. *Acta Crystallogr.* **1989**, *C45*, 1080–1082. (b) Hall, S. W.; Huffman, J. C.; Miller, M. M.; Avens, L. R.; Burns, C. J.; Arney, D. S. J.; England, A. F.; Sattelberger, A. P. *Organometallics* **1993**, *12*, 752–758. (c) Peters, R. G.; Scott, B. L.; Burns, C. J. *Acta Crystallogr.* **1999**, *C55*, 1482–1483.

(46) Bohrer, R.; Conradi, E.; Mueller, U. *Z. Anorg. Allg. Chem.* **1988**, *558*, 119–127.

(47) Levy, J. H.; Taylor, J. C.; Wilson, P. W. *J. Inorg. Nucl. Chem.* **1978**, *40*, 1055–1057.

(48) While no structurally characterized pentavalent uranium iodide complexes have been reported, bond lengths between ∼3.0 and 3.2 Å have been noted for other uranium oxidation states. For representative examples, see: (a) Avens, L. R.; Burns, C. J.; Butcher, R. J.; Clark, D. L.; Gordon, J. C.; Schake, A. R.; Scott, B. L.; Watkin, J. G.; Zwick, B. D. *Organometallics* **2000**, *19*, 451–457. (b) Crawford, M. J.; Mayer, P. *Inorg. Chem.* **2005**, *44*, 5547–5549. (c) Maynadié, J.; Berthet, J. C.; Thuéry, P.; Ephritikhine, M. *Organometallics* **2006**, *25*, 5603–5611.

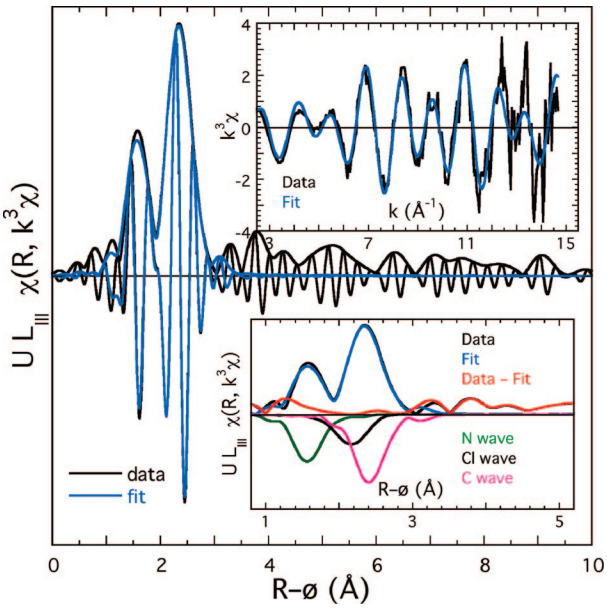

Figure 4. Raw uranium L_{III}-edge k^3-weighted EXAFS data (top inset), Fourier transform without phase corrections of the k^3-weighted EXAFS (middle), and curve-fitting analysis of the Fourier-transformed spectrum (bottom inset) for $(C_5Me_5)_2U(=N\text{-}2,4,6\text{-}{}^tBu_3\text{-}C_6H_2)(Cl)$ (**4**).

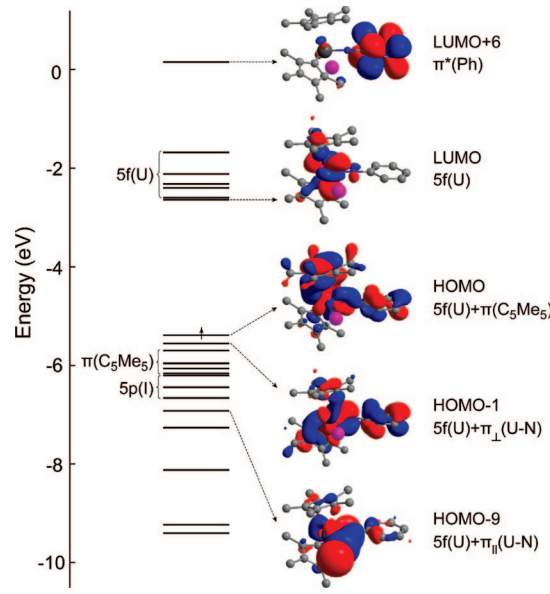

Figure 5. Occupied and virtual MO energy levels of $(C_5Me_5)_2U(=N\text{-}C_6H_5)(I)$ (**12**) and plots of orbitals with significant 5f or U=N bonding character (spin-up levels are shown with unpaired electron in HOMO).

However, solid-state structural information was obtained by analyzing the uranium L_{III}-edge X-ray absorption spectrum.[50] The background-subtracted k^3-weighted extended X-ray absorption fine structure (EXAFS) spectrum of **4** and the calculated fit are shown in Figure 4, as are the Fourier transform modulus and theoretical fit of the k^3-weighted EXAFS data, which were generated without phase corrections. The theoretical EXAFS modeling code, FEFF7,[51] was employed to calculate the backscattering phases and amplitudes of the individual neighboring atoms, using $(C_5Me_5)_2U(=N\text{-}2,6\text{-}{}^iPr_2\text{-}C_6H_3)(Cl)$ (**8**) as a model compound, and both the k^3-weighted $\chi(k)$ and $\chi(R)$ indicate a reasonable fit in both phase and amplitude.

The Fourier-transformed spectrum contains two large peaks, and although the first peak was fit with a single shell, the curve-fitting analysis revealed the second peak to be asymmetric, and it was fit with two shells. The first shell is attributed to the nitrogen atom with a U=N distance of 1.97(1) Å and is consistent with the formulation of a U=N_{imido} bond. This distance is similar to the U=N_{imido} distances observed for compounds **3**, **5**, **6**, **8**–**10**, which were determined by single-crystal X-ray crystallography. The second wave, which was fit with a single chloride atom, has a distance of 2.60(2) Å and is similar to the U−Cl distance (2.621(2) Å) in complex **8**. The final wave was attributable to the ring carbons of the pentamethylcyclopentadienyl ligand and fit with a U–C_5Me_5 distance of 2.84(1) Å. This average distance in **4** is significantly longer than the 2.75(4) Å average U–C_5Me_5 distance observed in $(C_5Me_5)_2U(=N\text{-}2,6\text{-}{}^iPr_2\text{-}C_6H_3)(Cl)$ (**8**) and is likely a manifestation of the steric demands of the $(=N\text{-}2,4,6\text{-}{}^tBu_3\text{-}C_6H_2)$ ligand compared to the $(=N\text{-}2,6\text{-}{}^iPr_2\text{-}C_6H_3)$ ligand.[52] The amplitude of the U−C wave was only approximated to half of that expected from the total number of ring carbons, which may be attributable to variation in the U–C_5Me_5 bond distances in **4**, resulting in an anharmonic distribution and the loss of amplitude. This is consistent with metrical parameters observed for compounds **3**, **5**, **6**, **8**–**10**, whose U–C_5Me_5 distances range from 2.70 to 2.90 Å. Although the data were of high enough quality to obtain bond distances for the uranium−imido, uranium−chloride, and U–C_5Me_5 interactions, the methyl groups on the C_5Me_5 ligand and the carbon atoms on the imido ligands were not resolvable.

Density Functional Calculations. The structures of the ground states of the model systems $(C_5Me_5)_2U(=N\text{-}C_6H_5)(F)$ (**11**) and $(C_5Me_5)_2U(=N\text{-}C_6H_5)(I)$ (**12**) were calculated using density functional theory (DFT) approaches. As can be seen in Table 2, there is good overall agreement (within 0.05 Å and 10°) between the calculated and experimental structures. The calculated U−X bond lengths for **11** and **12** are 2.117 Å (expt = 2.122(5) Å) and 3.064 Å (expt = 3.0116(6), 3.0385(7) Å), and the U=N distances are 1.969 Å (expt = 1.965(8) Å) and 1.944 Å (expt = 1.975(6), 1.974(7) Å), respectively. Likewise, **11** and **12** have N−U−X angles of 107.8° (expt = 97.0(3)°) and

(49) Compound **10** crystallized with two independent yet similar structures in the unit cell. Selected geometric parameters for one molcule are presented in Table 1, with those for the other being as follows: U−I = 3.0482(7) Å; U=N = 1.960(7) Å; N−C_{Ar} = 1.431(10) Å; N−U−X = 107.0(2) °; U=N−C_{Ar} = 165.9(6)°. For a complete list of bond distances and angles for complex **10**, see ref 23.

(50) For recent examples where EXAFS has been used to provide structural information, see: (a) Allen, P. G.; Bucher, J. J.; Clark, D. L.; Edelstein, N. M.; Ekberg, S. A.; Gohdes, J. W.; Hudson, E. A.; Kaltsoyannis, N.; Lukens, W. W.; Neu, M. P.; Palmer, P. D.; Reich, T.; Shuh, D. K.; Tait, C. D.; Zwick, B. D. *Inorg. Chem.* **1995**, *34*, 4797–4807. (b) Allen, P. G.; Shuh, D. K.; Bucher, J. J.; Edelstein, N. M.; Reich, T.; Denecke, M. A.; Nitsche, H. *Inorg. Chem.* **1996**, *35*, 784–787. (c) Clark, D. L.; Conradson, S. D.; Donohoe, R. J.; Keogh, D. W.; Morris, D. E.; Palmer, P. D.; Rogers, R. D.; Tait, C. D. *Inorg. Chem.* **1999**, *38*, 1456–1466. (d) Lukens, W. W., Jr.; Allen, P. G.; Bucher, J. J.; Edelstein, N. M.; Hudson, E. A.; Shuh, D. K.; Reich, T.; Andersen, R. A. *Organometallics* **1999**, *18*, 1253–1258. (e) Jiang, J.; Renshaw, J. C.; Sarsfield, M. J.; Livens, F. R.; Collison, D.; Charnock, J. M.; Eccles, H. *Inorg. Chem.* **2003**, *42*, 1233–1246. (f) Catalano, J. G.; Brown, G. E., Jr. *Geochim. Cosmochim. Acta* **2005**, *69*, 2995–3005. (g) Nikitenko, S. I.; Hennig, C.; Grigoriev, M. S.; Le Nauor, C.; Cannes, C.; Trubert, D.; Bossé, E.; Berthon, C.; Moisy, P. *Polyhedron* **2007**, *26*, 3136–3142.

(51) Ankudinov, A. L.; Rehr, J. J. *Phys. Rev. B: Condens. Matter* **1997**, *56*, R1712–R1715.

(52) Evans, W. J.; Kozimor, S. A.; Ziller, J. W. *Inorg. Chem.* **2005**, *44*, 7960–7969.

Table 2. Comparison of Calculated Geometric Parameters for Model Compounds $(C_5Me_5)_2U(=N\text{-}C_6H_5)(X)$ (X = F (**11**), I (**12**)) with Complexes **3**, **6**, and **10**

	$(C_5Me_5)_2U(=N\text{-}C_6H_5)(F)$ (**11**)		$(C_5Me_5)_2U(=N\text{-}C_6H_5)(I)$ (**12**)		
	expt, ^{t}Bu (**3**)	calcd	expt, ^{t}Bu (**6**)	expt, ^{i}Pr (**10**)	calcd
U−X (Å)	2.122(5)	2.117	3.0116(6)	3.0385(7)	3.064
U=N (Å)	1.965(8)	1.969	1.975(6)	1.974(7)	1.944
N−C_{Ar} (Å)	1.415(11)	1.376	1.418(8)	1.406(10)	1.380
U−$C_5Me_{5(cent)}$ (Å)	2.505	2.505, 2.502	2.528	2.459, 2.454	2.512, 2.510
N−U−X (°)	97.0(3)	107.8	97.20(16)	106.6(2)	97.22
U=N−C_{Ar} (°)	171.0(7)	176.9	169.7(5)	170.7(6)	175.2

97.22° (expt = 97.20(16)°, 106.6(2)°) and U=N−C_{Ar} angles of 176.9° (expt = 171.0(7)°) and 175.2° (expt = 169.7(5)°, 170.7(6)°), respectively. Presumably, the small overall deviations in bond angles can be largely attributed to the unfavorable steric interactions in the experimental structures with ^{t}Bu and ^{i}Pr substituents on the imido groups that are not present in the calculated model complexes.

The electronic structure of the U^V−imido halide complexes arises from the interactions of the pentamethylcyclopentadienyl, halide, and imido ligands with the uranium metal center. The multiple bond formed between the imido ligand and the uranium center can be viewed by considering a formal dianionic $[N\text{-}C_6H_5]^{2-}$ fragment interacting with the uranium 6d and 5f orbitals. A primary σ donation from the $[N\text{-}C_6H_5]^{2-}$ fragment to the metal center, coupled with two π interactions, results in a nearly linear (U=N−C_{Ar} = 176.9° and 175.2°, calculated) bonding interaction between the imido ligand and the uranium metal center. The first imido nitrogen π lone pair is conjugated with the imido aryl group to form a U=N $\pi_\perp$ bond, while the second lone pair lies in the plane of the aryl ring forming a U=N $\pi_{||}$ bond. This interpretation is similar to that from calculations[53] determined for the model system $(C_5H_5)_2U(=N\text{-}C_6H_5)_2$ utilized in describing the bonding for the previously reported U^{VI}−bis(imido) complex, $(C_5Me_5)_2U(=N\text{-}C_6H_5)_2$.[38] A more recent investigation by Belkhiri and co-workers on the bonding analysis of the actinide−imido bond in $(C_5H_5)_2An(=N\text{-}C_6H_5)_2$ (An = Th, U) and related systems also noted the importance of the participation of 5f orbitals in σ and π interactions to form the coplanar U=N-C_6H_5 group.[54] In the same report, it was also observed that the transition metal−imido bond in Mo(VI) complexes cannot achieve the analogous triple bond nature utilizing only d-orbitals, and as a result the Mo=N−C_{Ar} angle is close to 150°.

The occupied and virtual MO energy levels are depicted schematically in Figure 5, where selected orbitals are plotted, and analysis of the highest occupied orbitals in the complexes is presented in Table 3, where the amount of 5f and 6d admixture on the uranium metal center is given along with the N_{imido} and halide components. The HOMO contains the unpaired 5f electron, but has a considerable ligand component. The HOMO−2 for **12** shows strong U=N ($\pi_\perp$) π bonding character and 5f (19%) and 6d (5%) admixture. Below this orbital are four occupied π orbitals corresponding to two pairs of the set from the C_5Me_5 ligands as well as the three iodide lone pair 5p orbitals. The MOs show considerable mixing of the various contributions from different ligands, and, as a result, it is difficult to isolate one metal–ligand combination in any particular orbital. The U=N ($\pi_{||}$) bond is particularly evident in HOMO−9, where some U−I bonding character also exists. The resulting energy level diagram for the fluoride complex **11** is similar, except that the fluoride ligand lone pairs occur at much lower energies (–10.3 to –9.8 eV in **11** vs –7.2 to –6.2 eV in **12**).

Table 3. MO Components for the f^1 Complexes $(C_5Me_5)_2U(=N\text{-}C_6H_5)(F)$ (**11**) and $(C_5Me_5)_2U(=N\text{-}C_6H_5)(I)$ (**12**)

$(C_5Me_5)_2U(=N\text{-}C_6H_5)(F)$ (**11**)						$(C_5Me_5)_2U(=N\text{-}C_6H_5)(I)$ (**12**)					
MO	*E* (eV)	U_{6d}	U_{5f}	N	F	MO	*E* (eV)	U_{6d}	U_{5f}	N	I
L+6	0.27		1			L+6	0.15		3		
L+5	−1.38		85			L+5	−1.68		87		
L+4	−1.72		68	8		L+4	−2.12		80		
L+3	−2.02		92			L+3	−2.32		70		
L+2	−2.07		94			L+2	−2.40		94		
L+1	−2.10		77			L+1	−2.60		85		
LUMO	*−2.29*		*92*			*LUMO*	*−2.64*		*90*		
HOMO	*−5.18*		*33*	*17*		*HOMO*	*−5.39*		*42*	*3*	
H−1	−5.35		11	2		H-1	−5.56		37	13	
H−2	−5.49		73			H-2	−5.70	5	19	8	
H−3	−5.59	5	3	9		H-3	−5.96	4	14		21
H−4	−5.99	10	13		1	H-4	−6.06	3	37		15
H−5	−6.11	7	31			H-5	−6.16	9	7		20
H−6	−6.43	14	14	49		H-6	−6.20	2	8		71
H−8	−7.87	4	3	30		H-7	−6.44	11			58
H−14	−9.02	4	1	7	3	H-9	−6.92	15	5	25	39
H−16	−9.19	2	1	10	2	H-10	−7.26	12	18	14	48
H−21	−9.84	2	2		39	H-11	−8.12	4	5	31	
H−23	−9.93	4	2	2	53	H-17	−9.23	6	1	4	
H−26	−10.35	7	3	4	61	H-19	−9.40	2	2	12	
H−27	−10.57	2	2	8	13	H-27	−10.66	4	2	15	

Table 4. Net Spin and Charge Distribution for $(C_5Me_5)_2U(=N\text{-}C_6H_5)(F)$ (**11**) and $(C_5Me_5)_2U(=N\text{-}C_6H_5)(I)$ (**12**) and the Corresponding Anions ([**11**]$^-$ and [**12**]$^-$) and Cations ([**11**]$^+$ and [**12**]$^+$)

	U	N	C	X (I, F)
		Net Spin		
11	+1.38	−0.19	+0.04	−0.01
[**11**]$^-$	+2.18	−0.11	+0.01	−0.01
12	+1.44	−0.20	+0.04	−0.02
[**12**]$^-$	+2.20	−0.11	+0.02	−0.01
		Charges		
11	+1.17	−0.64	+0.21	−0.47
[**11**]$^+$	+1.14	−0.58	+0.20	−0.43
[**11**]$^-$	+1.14	−0.69	+0.22	−0.52
12	+0.95	−0.63	+0.21	−0.46
[**12**]$^+$	+0.87	−0.58	+0.19	−0.26
[**12**]$^-$	+1.02	−0.68	+0.21	−0.66

The calculated spin densities (Table 4) reflect the $5f^1$ configuration on the uranium(V) metal center in these complexes. The Mulliken analysis shows 1.38 unpaired electrons on the uranium atom for **11** and 1.44 for **12**, somewhat higher than the formal spin of one unpaired electron. Small amounts of opposite spins arise on the nitrogen atom involved in forming a multiple bond with the metal. The halide atom and the aryl group on the imido ligand exhibit no spin density. These results show that the spin properties are not wholly described by the HOMO (or SOMO) from the DFT calculations, which has only 33% (**11**) and 42% (**12**) metal character, but that there are

Table 5. Flow of Charge upon Oxidation or Reduction of $(C_5Me_5)_2U(=N\text{-}C_6H_5)(F)$ (**11**) and $(C_5Me_5)_2U(=N\text{-}C_6H_5)(I)$ (**12**) from Mulliken Analysis

	U	X	N	Ph	C_5Me_5	sum
11 → $[\mathbf{11}]^+$	−0.022	+0.042	+0.056	+0.206	+0.360, +0.358	+1.000
11 → $[\mathbf{11}]^-$	−0.031	−0.049	−0.052	−0.231	−0.313, –0.324	−1.000
12 → $[\mathbf{12}]^+$	−0.088	+0.209	+0.047	+0.172	+0.330, +0.329	+1.000
12 → $[\mathbf{12}]^-$	+0.033	−0.185	−0.049	−0.208	−0.299, –0.291	−1.000

Table 6. Comparison of Calculated Geometric Parameters for $(C_5Me_5)_2U(=N\text{-}C_6H_5)(X)$ (X = F (**11**), I (**12**)) and Their Corresponding Cations and Anions

	$(C_5Me_5)_2U(=N\text{-}C_6H_5)(F)$ (**11**)			$(C_5Me_5)_2U(=N\text{-}C_6H_5)(I)$ (**12**)		
	charge = 0	charge = +1	charge = −1	charge = 0	charge = +1	charge = −1
U−X (Å)	2.117	2.084	2.170	3.064	2.958	3.212
U=N (Å)	1.969	1.926	2.022	1.944	1.909	1.994
$N-C_{Ar}$ (Å)	1.376	1.380	1.358	1.380	1.384	1.365
$U-C_5Me_{5(cent)}$ (Å)	2.505, 2.502	2.449, 2.449	2.582, 2.588	2.512, 2.510	2.468, 2.471	2.581, 2.580
N−U−X (°)	107.8	101.1	104.1	97.22	93.9	100.0
$U=N-C_{Ar}$ (°)	176.9	172.2	179.6	175.2	173.4	178.6

additional contributions to the net spin polarization from other occupied orbitals.

The next six orbitals of the virtual set (LUMO, LUMO+1 to LUMO+5) correspond to the other 5f orbitals, thereby completing the manifold of the f levels. The first orbital beyond this group (LUMO+6) corresponds to the π^* orbital of the imido aryl group. In terms of the electronic absorption spectra, this leads to the qualitative picture of low-lying f−f states as the lowest excitations for the molecule. Other excitations could involve ligand-to-metal 5f excitations and, at higher energies, ligand-based excitations involving the virtual π^* orbitals. Preliminary spectroscopic assignments are discussed below in the Electronic Spectroscopy section. In order to get a qualitative picture of the energies involved in the f−f states including spin–orbit coupling, a simple ligand field calculation was performed. The preliminary results show a set of three closely spaced Kramers doublet levels between 0 and 2800 cm^{-1}, and a second set of four doublets between 6200 and 10000 cm^{-1}, with the first two levels occurring at 6200 and 7100 cm^{-1}, suggesting that two peaks in this region may be arising from distinct electronic origins (*vide infra*).

Cation and anion calculations were performed for both $(C_5Me_5)_2U(=N\text{-}C_6H_5)(F)$ (**11**) and $(C_5Me_5)_2U(=N\text{-}C_6H_5)(I)$ (**12**) in order to understand their structural, electronic, spin, and redox properties. The metrical parameters for the corresponding cations ($[\mathbf{11}]^+$ and $[\mathbf{12}]^+$) and anions ($[\mathbf{11}]^-$ and $[\mathbf{12}]^-$) are essentially identical to their neutral counterparts (Table 6). While the bond lengths are slightly shorter for the cationic species and marginally longer for anionic complexes compared to those of the corresponding neutral parent species, the geometrical parameters are generally unaffected by the removal or addition of one electron. Note that this finding agrees well with experiment, as noted above, with the U=N bond length in particular being noticeably insensitive to metal oxidation state.

The formation of the anions $[\mathbf{11}]^-$ and $[\mathbf{12}]^-$ corresponds to a $5f^2$ configuration on the uranium metal, giving U^{IV}. The added electron is largely localized in the f-orbital on the uranium center and comprised entirely of 5f character, which was verified by investigating the ground-state natural orbitals (NOs). The calculations indicate a higher spin, 2.18 and 2.20 unpaired electrons, for $[\mathbf{11}]^-$ and $[\mathbf{12}]^-$, respectively (Table 4). Compared to the neutral complexes (**11** and **12**) the spins of the negative ions have added about 0.8 electron to the metal, with the remainder of the unpaired spin (0.2 e^-) delocalized throughout the C_5Me_5 rings. As can be seen in Table 5, it is also interesting to note that the Mulliken charges on the uranium center and imido functional groups are essentially constant, regardless of whether an electron is added or removed. For the case of adding an electron, the additional charge goes partially to the halogen (0.05 electron for fluoride $[\mathbf{11}]^-$, 0.2 electron for iodide $[\mathbf{12}]^-$), with ∼0.3 electron to each C_5Me_5 ligand and 0.2 electron onto the imido ligand. Similar results were provided by the NBO analysis of natural charges.[55]

To evaluate the relative U^V/U^{IV} redox potentials for the U^V−imido complexes, calculations were performed for their negative ions as gas-phase species. The electron affinity of **12** is greater than that for **11**, as shown by the relative energy of the anion $[\mathbf{12}]^-$ (−2.20 eV) compared to that of the anion $[\mathbf{11}]^-$ (−1.73 eV). This result is consistent with the experimental observations that the U^V−imido iodide complexes have more positive reduction potentials than the corresponding U^V−imido fluoride complexes (see Table 7). The calculations for the cations $[\mathbf{11}]^+$ and $[\mathbf{12}]^+$ show essentially no difference between the U^{VI}/U^V redox potentials for **11** and **12** (within 0.03 eV). Inclusion of zero-point energy corrections at 298 K, enthalpy corrections, and solvation effects has little effect on the potential of the U^{VI}/U^V redox couples; the two potentials remain within 0.02 eV difference. Experimentally, the U^{VI}/U^V redox potentials show much less variation across the halide series than do U^V/U^{IV} redox potentials (*vide infra*).

Electrochemistry. Cyclic and square-wave voltammetric data were collected for all U^V−imido halide complexes in ∼0.1 M $[Bu_4N][fluoroarylborate]$/tetrahydrofuran solution ([fluoroarylborate] = $[B(C_6F_5)_4]^-$ or $[B(3,5\text{-}(CF_3)_2\text{-}C_6H_3)_4]^-$). Most data were collected at room temperature; however, complex **7** was found to decompose within tens of minutes in these solvent/electrolyte solutions. Thus, investigations of the scan-rate-dependent behavior in the cyclic voltammetry for this complex were conducted at approximately –50 °C. Typical cyclic voltammograms are illustrated in Figure 6. Each complex

(53) Hay, P. J. *Faraday Discuss.* **2003**, *124*, 69–83.
(54) Belkhiri, L.; Lissillour, R.; Boucekkine, A. *THEOCHEM* **2005**, *757*, 155–164.
(55) Glendening, E. D.; Badenhoop, J. K.; Reed, A. E.; Carpenter, J. E.; Bohmann, J. A.; Morales, C. M.; Weinhold, F. *NBO 5.0*; Theoretical Chemistry Institute, University of Wisconsin: Madison, WI, 2001.

Table 7. Summary of Redox Potential Data[a] for $(C_5Me_5)_2U(=N-Ar)(X)$ Complexes **3**–**10** in ∼0.1 M $[Bu_4N]$[fluoroarylborate][b]/THF Solution at Room Temperature

U^V complexes	Ar	X	electrolyte anion[b]	$E_{1/2}(U^{VI}/U^V)$ (V)	$E_{1/2}(U^V/U^{IV})$ (V)	$\Delta E_{1/2}$ (V)
3	2,4,6-^{t}Bu$_3$-C_6H_2	F	BAr_F	−0.19	−1.78	1.59
4	2,4,6-^{t}Bu$_3$-C_6H_2	Cl	BAr_F	0.04	−1.50	1.54
5	2,4,6-^{t}Bu$_3$-C_6H_2	Br	$B(C_6F_5)_4$	0.04	−1.43	1.47
6	2,4,6-^{t}Bu$_3$-C_6H_2	I	BAr_F	0.04	−1.25	1.29
7[c]	2,6-^{i}Pr$_2$-C_6H_3	F	BAr_F	−0.14	−1.81	1.67
8	2,6-^{i}Pr$_2$-C_6H_3	Cl	BAr_F	0.03	−1.52	1.55
9	2,6-^{i}Pr$_2$-C_6H_3	Br	BAr_F	0.07	−1.44	1.51
10	2,6-^{i}Pr$_2$-C_6H_3	I	$B(C_6F_5)_4$	0.11	−1.37	1.48
					$\lvert\Delta E_{1/2}\rvert_{(av)}$	1.51 ± 0.04

U^{IV} precursors	Ar	electrolyte anion[b]	$E_{1/2}(U^V/U^{IV})$ (V)	$E_{1/2}(U^{IV}/U^{III})$ (V)	$\Delta E_{1/2}$ (V)
1[d]	2,4,6-^{t}Bu$_3$-C_6H_2	$B(C_6F_5)_4$	−0.73	−2.61	1.88
2[e]	2,6-^{i}Pr$_2$-C_6H_3	BAr_F	−0.86	−2.40	1.54

[a] All $E_{1/2}$ values are versus $[(C_5H_5)_2Fe]^{+/0}$ and were determined from the peak position in a square-wave voltammogram or from the average of the cathodic and anodic peaks in a cyclic voltammogram. [b] Electrolyte anion was either $[B(3,5\text{-}(CF_3)_2\text{-}C_6H_3)_4]^-$ (BAr_F) or $[B(C_6F_5)_4]^-$ ($B(C_6F_5)_4$). [c] Although scan-rate-dependent behavior was explored at ∼−50 °C, potential calibration data were collected for this complex at room temperature using a freshly prepared solution. [d] Data from ref 20. [e] Data from ref 23.

exhibits one oxidation wave, attributed to the U^{VI}/U^V redox process, and one reduction wave, attributed to the U^V/U^{IV} redox process. The only other voltammetric activity seen in these systems occurs at ∼1 V (vs $[(C_5H_5)_2Fe]^{+/0}$) and is ascribed to irreversible C_5Me_5-based oxidation, as noted in previous investigations.[9,20] In particular, there are no clear indications of any oxidation processes attributable to the coordinated halide ligands, although the irreversible nature of the nominal C_5Me_5-based processes could easily mask additional halide-based redox transformations. Finally, there were no additional metal-based reduction processes (e.g., U^{IV}/U^{III} as seen in previous studies of uranium(IV) metallocenes[9,20]) resolved for the U^V−imido complexes within the negative potential range of these solvent/electrolyte systems. The redox potential data derived from the voltammetric experiments are summarized in Table 7.

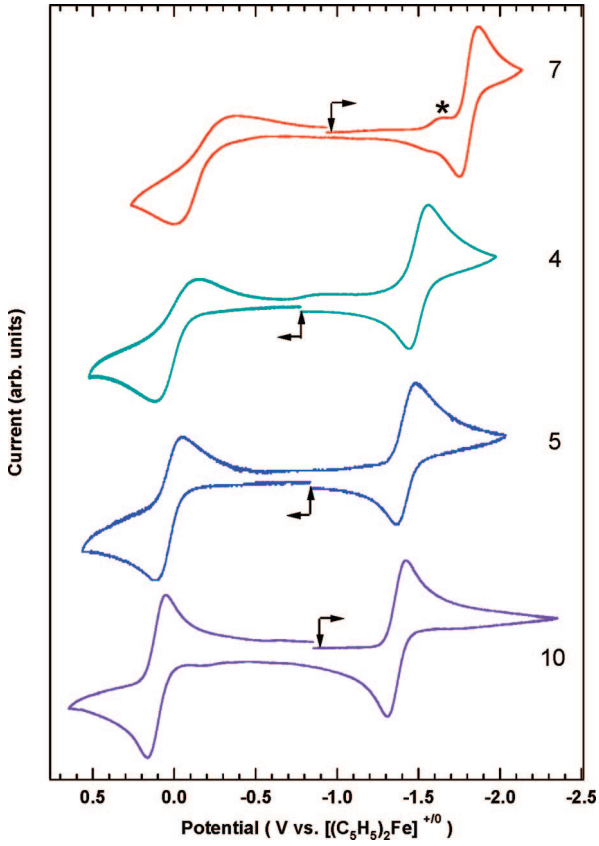

Figure 6. Cyclic voltammograms for $(C_5Me_5)_2U(=N-Ar)(X)$ complexes **4**, **5**, **7**, and **10** in ∼0.1 M $[Bu_4N]$[fluoroarylborate]/THF solution at 200 mV/s scan rate and at room temperature for all complexes except **7**, for which $T \approx -50$ °C. The low-current signal marked with an asterisk in the scan of **7** is believed to be due to a small amount of **8** present as an impurity. Vertical arrows indicate the initial (rest) potential, and horizontal arrows indicate the initial scan direction.

The observed redox behavior of these complexes provides direct insight into the generic influence ligation of the halide ion (F^-, Cl^-, Br^-, or I^-) to the $(C_5Me_5)_2U(=N\text{-}Ar)$ core plays on the redox energetics in these bent metallocene complexes. Further, it enables assessment of the more subtle impact of changing the halide ion from fluoride through iodide in these structures. In comparison to their U^{IV}−imido precursors, the U^V/U^{IV} couple for all the U^V−imido halide complexes is shifted to more negative potentials (destabilized) by ∼1 V, and, in contrast to the behavior of the U^{IV}−imido precursors and other tetravalent uranium bent metallocene complexes,[9,20,23] the U^{VI}/U^V couple emerges within the available potential window, indicating a significant stabilization of the U^{VI} oxidation state in the halide complexes. These two gross perturbations in the redox behavior across the entire suite of U^V−imido halide complexes are the principal manifestations of halide ion complexation on the $(C_5Me_5)_2U(=N\text{-}Ar)$ core.

The variations in redox potentials that are specific to the identity of the halide ion across this series of complexes are found to be more subtle, and, as seen in Table 7, they are more pronounced on the $E_{1/2}$ values for the reduction process than those of the oxidation process. Nonetheless, for both the ^{t}Bu− and ^{i}Pr−imido series, there are consistent trends in the $E_{1/2}$ values for both the oxidation process and the reduction process according to $E_{1/2}(F^-) < E_{1/2}(Cl^-) < E_{1/2}(Br^-) < E_{1/2}(I^-)$, with the exception of the oxidation process for the ^{t}Bu−imido series, for which the half-wave potential remains constant for X = Cl, Br, and I. These results are remarkably consistent with those predicted from the DFT calculations for the model complexes $(C_5Me_5)_2U(=N\text{-}C_6H_5)(F)$ (**11**) and $(C_5Me_5)_2U(=N\text{-}C_6H_5)(I)$ (**12**). Specifically, theory predicts that **11** should be more difficult to reduce (have a lower electron affinity) than **12**, while the oxidation potential (ionization potential) is predicted to be roughly equal for the two halide complexes. This trend in redox potentials versus halide ion ligation at first might seem counterintuitive on the basis of the relative electronegativities of the halide ions and the inductive influence this might be expected to exert on the electron density at the redox-active metal center. We attribute the observed trend to a greater degree of polarizability of the halide orbitals with increasing atomic number of the halide that more readily accommodates the addition of electrons in the principally metal-based orbitals in the heavier halide complexes.

A final observation on the thermodynamic properties of these U^V−imido halide complexes revealed in the voltammetric data is the nearly constant spacing between the metal-based oxidation and reduction processes across this entire series of eight complexes: $\Delta E_{1/2} = 1.51 \pm 0.04$ V (Table 7). A similar consistency in separation has been found between metal-based oxidation (U^{IV}/U^V) and reduction (U^{III}/U^{IV}) processes for a

broad range of $(C_5Me_5)_2U^{IV}L$ and $(C_5Me_5)_2U^{IV}L'_2$ (L = imide, L′ = ketimide, hydrozanate) complexes, but in these tetravalent systems this consistency in separation between oxidation and reduction waves is on average ~2.1 V.[9,20] The constancy in these average values implies that attractive (electron−nucleus) and repulsive (electron–electron) interactions, not specific perturbations introduced by the ligand sets in the metallocene wedge, are the dominant factors in determining the relative redox energetics, but we are unaware of evidence for these trends in other actinide systems.

The cyclic voltammetric experiments provide one additional interesting result. As illustrated in Figure 6 for cyclic scans collected at 200 mV/s and confirmed in the more detailed scan-rate-dependent behavior (not shown), the U^V−imido complexes all exhibit markedly different heterogeneous electron-transfer rate constants (k_{et}) for the metal-based oxidation vs reduction processes. In particular, the oxidation process is always found to be more sluggish than the reduction process, as evidenced by the greater separation between the anodic and cathodic peaks for the oxidation wave compared to the reduction wave. No attempt was made to quantify these electron-transfer rate constants because of inherent problems in completely accounting for contributions from uncompensated resistance in these relatively low dielectric solutions. Nonetheless, it is clear even from the data in Figure 6 that the effect varies from complex to complex, with the difference in $k_{et}(U^{VI}/U^V)$ versus $k_{et}(U^V/U^{IV})$ being greatest for the fluoride complexes (**3** and **7**) and least for the iodide complexes (**6** and **10**). The DFT results described above (Table 6) do not indicate any substantially greater change in the coordination environment about the metal ion for the oxidation step versus the reduction step to which one could attribute a difference in the rate constants associated with inner-sphere structural reorganization. However, we believe this effect is a manifestation of the greater structural compensation required to accommodate metal ion size reduction ($U^V \rightarrow U^{VI}$) than that of metal ion size expansion ($U^V \rightarrow U^{IV}$) in these complexes.

Electronic Spectroscopy. The organometallic U^V−imido halide complexes provide two important opportunities to explore electronic structure. The first pertains to the relatively uncommon $5f^1$ valence electronic configuration possessed by these systems. Systems with a single 5f-electron (Pa^{4+}, U^{5+}, Np^{6+}) constitute the simplest examples to explore spin–orbit versus crystal-field effects since there are no electron–electron repulsion terms to consider and the f-orbital density of states is reduced to only two manifolds, a $^2F_{5/2}$ ground-state manifold and a $^2F_{7/2}$ excited-state manifold, whose individual multiplet levels will split in response to the symmetry and strength of the field induced by the ligands. Thus, for these $(C_5Me_5)_2U(=N\text{-}Ar)(X)$ complexes, the electronic transitions between states derived from these manifolds (f−f or ligand-field transitions) provide direct insight into ligand-field strengths from both imido and halide ligands for an approximately fixed spin–orbit coupling interaction associated with uranium(V) in this coordination environment. The second opportunity derives from the existence of occupied and virtual ligand-based orbitals derived from the imido ligand that lie close in energy to the metal valence orbitals, as discussed in the DFT section. This engenders the formation of new molecular electronic states of ligand-localized and metal–ligand charge-transfer character similar to those found in early transition-metal−imido complexes and from which the degree of covalent metal–ligand bonding interactions can be inferred from electronic spectral data involving transitions between these states.

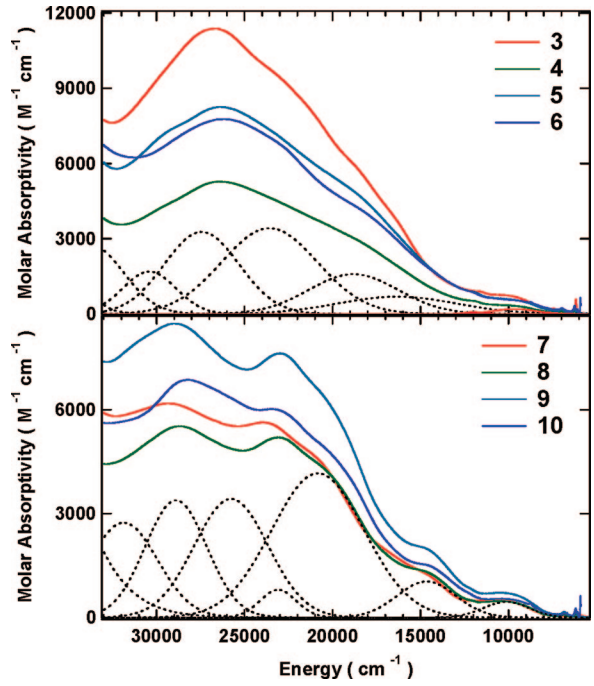

Figure 7. UV–visible−NIR absorption spectra of $(C_5Me_5)_2U(=N\text{-}Ar)(X)$ complexes **3**–**6** (top) and **7**–**10** (bottom) in toluene solution at room temperature. Dashed lines are component bands from Gaussian fit of spectra for complexes **4** and **8**.

The room-temperature electronic absorption spectra over the entire accessible energy range (determined by properties of the toluene solvent) for all eight U^V−imido halide complexes are illustrated in Figure 7. These spectra are clearly dominated by broad, relatively intense bands over the entire spectral range, but weaker and narrower bands typical of f−f transitions can be readily seen in the lower energy region. To provide some gauge of spectral band components in the broadband portions of the spectra, the spectral region above ~7000 cm^{-1} has been fit using the minimum number of Gaussian profiles required to adequately reproduce the observed spectra. Examples of the component bands from these fitting results are highlighted for complexes **4** and **8** in Figure 7. It is noteworthy that the total spectral band profile over the entire energy range is quite similar for all ^{t}Bu−imido complexes (**3**–**6**) and for all ^{i}Pr−imido complexes (**7**–**10**), although there are changes in the molar absorptivities that certainly exceed the uncertainty in these measurements.[56]

Specific and detailed assignments of all the broad bands reflected in the Gaussian fits to these spectra are not possible on the basis of existing information. However, the DFT results described above and published data for early transition-metal−imido complexes can be used to suggest plausible generic assignments for this portion of the spectra. While we know of no reports of spectroscopic data for d^1 imido systems to which we can compare our results, there are numerous d^0 imido systems for which detailed assignments are available.[57,58] The lowest-energy electronic transitions seen in transition-metal−imido complexes such as $(dme)Cl_3Ta(=N\text{-}R)$ (dme = dimethoxy-

(56) Uncertainties in the molar extinction coefficients are determined from the accuracy in weighing the complexes (milligram quantities) in the glovebox to prepare sample solutions and are estimated to be ±20%.
(57) Heinselman, K. S.; Hopkins, M. D. *J. Am. Chem. Soc.* **1995**, *117*, 12340–12341.
(58) Williams, D. S.; Korolev, A. V. *Inorg. Chem.* **1998**, *37*, 3809–3819.

ethane; R = alkyl or aryl) have been assigned to the electric-dipole-allowed singlet and triplet components of the $\pi_{M=N} \rightarrow nb_d$ (nb_d = nonbonding metal d orbital) charge-transfer transition. DFT results described in Figure 5 suggest that, among the set of valence orbitals for these uranium(V)−imido complexes, there are also high-lying occupied orbitals comprised principally of $\pi_{M=N}$ character (HOMO−1) and low-lying unoccupied orbitals of nonbonding f-orbital character (LUMO) that could give rise to similar $\pi_{M=N} \rightarrow nb_{5f}$ charge-transfer transitions. In the case of these $5f^1$ systems, the spin assignments for these charge-transfer transitions would be quartet and doublet (instead of triplet and singlet), but the relative intensities in the pair of transitions [$I_{(\text{triplet or quartet})} < I_{(\text{singlet or doublet})}$] should carry over to the $5f^1$ case. Thus, consistent with both DFT calculations and in analogy to transition-metal−imido systems, we propose that the bands at ∼10000 and ∼14000 cm^{-1} are $^4(\pi_{M=N} \rightarrow nb_{5f})$ and $^2(\pi_{M=N} \rightarrow nb_{5f})$ transitions, respectively. The relatively low oscillator strengths in these charge-transfer transitions are entirely consistent with the expected relatively small orbital overlap between the donor ($\pi_{M=N}$) and acceptor (5f) charge-transfer orbitals compared to that found in the transition-metal analogues.

The bands that lie to higher energy of the putative $\pi_{M=N} \rightarrow nb_{5f}$ charge-transfer transitions have substantially greater oscillator strength, suggesting that a different electronic transition is operative. Again, with recourse to the DFT results, we note that there is a virtual π^*_{Ph} orbital (LUMO+6) that lies to higher energy than the nb_{5f} orbital manifold. Thus, it is plausible that at least some the higher-energy bands in these spectra can be attributed to transitions of $\pi_{M=N} \rightarrow \pi^*_{Ph}$ character. Several such transitions, occurring at slightly different energies but having this same orbital description, would be possible for these complexes because of the existence of two discrete $\pi_{M=N}$ bonds (*vide supra*), although the intensities should differ in a manner that reflects the orthogonality of the two $\pi_{M=N}$ bonds and the impact this has on the allowedness of the $\pi \rightarrow \pi^*$ transition.

One further important observation from the broadband spectral data is that there does not appear to be any significant sensitivity to the identity of the halide ion. Thus, other than changes in molar absorptivity noted above, the spectra for the entire series of ^{t}Bu−imido complexes (**3–6**) look very similar, as do the spectra for all the ^{i}Pr−imido complexes (**7–10**). Fully allowed halide ligand-to-metal charge-transfer transitions are a common feature in the spectroscopy of uranium halide complexes.[59] Thus, the insensitivity in the spectral data to the identity of the halide indicates that any electronic transitions involving the halide ions, e.g., the halide-to-metal charge-transfer band(s), must lie to higher energy than probed in our experiments or have insufficient oscillator strengths to impart distinct features on top of the existing spectral bands.

The remaining important elements in these spectral data are the low-energy, low-intensity, narrow-band features that are just discernible in the data shown in Figure 7 and are ascribed to the f−f or ligand-field transitions. To accentuate this spectral region, the lowest-energy Gaussian bands from the fits described above were used to define the sloping tails that underlie these f−f bands. These Gaussian bands were subtracted from the total spectral envelopes in the energy region from ∼9000 to 5000 cm^{-1} to isolate the contributions from the f−f bands. Results

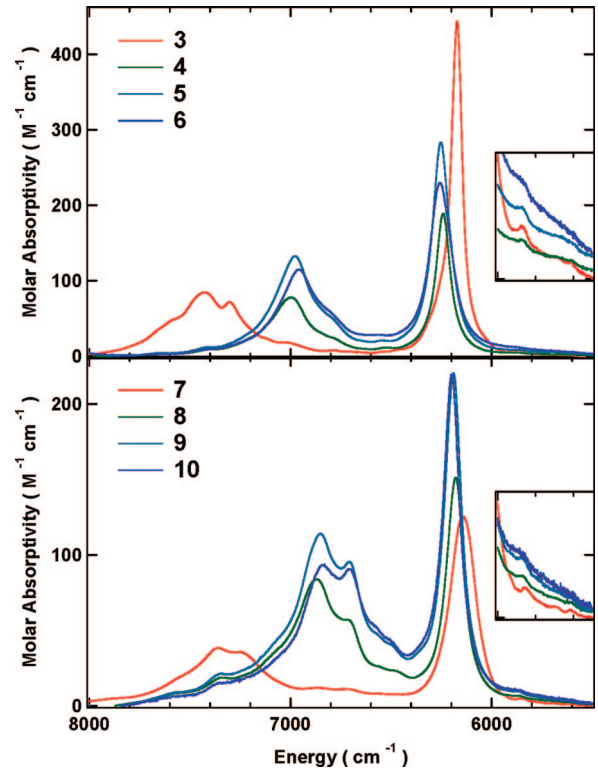

Figure 8. NIR absorption spectra of $(C_5Me_5)_2U(=N\text{-}Ar)(X)$ complexes **3–6** (top) and **7–10** (bottom) in toluene-d_8 solution at room temperature. Insets show expansions of vertical scale to illustrate vibronic hot bands.

from this operation are indicated in Figure 8 for all eight imido halide complexes. Note that data in this spectral region were collected in toluene-d_8 in 1 mm path length cells to minimize interference from the strong solvent vibrational overtone and combination bands. The resulting spectra are characterized by what appear to be two sets of bands, and there is now a very clear sensitivity in the spectra to the identity of both the halide ion and the imido ligand.

While there is not a large body of literature relating to spectroscopic characterization of $5f^1$ systems, there have been several detailed treatments of results for octahedral or pseudo-octahedral hexahalide complexes, particularly of U^V and Pa^{IV}.[15,60–65] These reports provide a framework within which we can begin to interpret the f−f spectral data for these U^V−imido systems. As noted above, spin–orbit coupling interactions will split the f-orbital manifold in an f^1 system into two subsets: a $^2F_{5/2}$ ground-state manifold and a $^2F_{7/2}$ excited-state manifold. The influence of an octahedral or pseudo-octahedral crystal field as in the hexahalide complexes will be to further lift the degeneracy within each manifold, giving rise to a total of five states in rigorous octahedral symmetry (Γ_7, Γ_8, $\Gamma_{7'}$, $\Gamma_{8'}$, and Γ_6 from lowest to highest energy using the conventional double-group notations in the O_h point group), two of which (Γ_8 and $\Gamma_{8'}$) are orbitally two-fold degenerate. A total of four electronic transitions would thus be expected in O_h

(59) Liu, G.; Beitz, J. V. Optical Spectra and Electronic Structure. In *The Chemistry of the Actinide and Transactinide Elements*, 3rd ed.; Morss, L. R., Edelstein, N. M., Fuger, J., Eds.; Springer: The Netherlands, 2006; Vol. 3, pp 2013–2111.

(60) Edelstein, N.; Brown, D.; Whittaker, B. *Inorg. Chem.* **1974**, *13*, 563–567.
(61) Karraker, D. G. *Inorg. Chem.* **1964**, *3*, 1618–1622.
(62) Penneman, R. A.; Sturgeon, G. D.; Asprey, L. B. *Inorg. Chem.* **1964**, *3*, 126–129.
(63) Reisfeld, M. J.; Crosby, G. A. *J. Mol. Spectrosc.* **1963**, *10*, 232–234.
(64) Reisfeld, M. J.; Crosby, G. A. *Inorg. Chem.* **1965**, *4*, 65–70.
(65) Selbin, J.; Ortego, J. D.; Gritzner, G. *Inorg. Chem.* **1968**, *7*, 976–982.

symmetry, and for crystalline $Cs[UF_6]$, for which the most attention has been devoted, these electronic transitions (and/or their non-totally symmetric vibronic components, since pure electronic transitions are dipole forbidden in rigorous O_h symmetry) have been identified to lie at ~4600, 6900, 12700, and 14200 cm^{-1}.[64]

The $(C_5Me_5)_2U(=N\text{-}Ar)(X)$ complexes **3**–**10** have at best C_s symmetry. This C_s crystal field environment results in complete lifting of the orbital degeneracies in the spin–orbit manifolds, yielding a total of seven states from which six electronic transitions would be expected. In addition, in this low-symmetry, non-centrosymmetric environment, the electric dipole selection rules are relaxed, and one might expect that the pure electronic transitions are able to carry substantial intensity. As noted in the theory discussion above, a simple ligand-field calculation that explicitly incorporates spin–orbit coupling for the model complexes $(C_5Me_5)_2U(=N\text{-}C_6H_5)(X)$ (X = F (**11**), I (**12**)) results in the prediction of two groups of energy levels: the first is comprised of the ground-state level and two additional levels within ~2800 cm^{-1} of the ground state, and the second is comprised of the four remaining levels that lie in the region between 6000 and 10000 cm^{-1} above the ground state. Notably, the two lowest-lying levels in this second group were predicted to be 6200 and 7100 cm^{-1} above the ground-state level.

As can be seen in Figure 8, there appear to be two sets of bands. The first set is comprised of an intense band in the region of ~6200 cm^{-1} for all complexes, the peak energy of which varies with halide ion (*vide infra*), and several much weaker bands to higher energy that are likely vibronic in character. This first set of bands also contains several very weak features on the low-energy side of the most intense band (inset, Figure 8). Data collected for these systems at 77 K, which will be presented in more detail in a forthcoming paper that will include additional discussion of the vibronic structure in these spectra, clearly show that these weak features at lower energy disappear at low temperature, indicating that they are vibronic hot bands. Thus, we propose that the most intense feature in this first set, at ~6200 cm^{-1}, is an electronic origin transition. The energy of this band is in excellent agreement with that predicted from simple ligand-field/spin–orbit calculations noted above. The second set of bands contains greater vibronic structure than the first set, and the low-temperature data are less helpful in identifying what the likely electronic origin band might be. Nonetheless, it is notable that this collection of bands occurs in approximately the same energy range (~7000 cm^{-1}) as the simple theoretical calculations predicted for the next higher-lying electronic transition. Of the remaining four electronic transitions that should be found in these complexes under this low-symmetry crystal field, we note that the two that are predicted to lie below ~3000 cm^{-1} would not be observed in our experiments because of strong solvent interferences, and the remaining two, predicted to lie at energies in the range from ~7000 to 10000 cm^{-1}, could be masked by the more intense charge-transfer bands that tail well into this NIR spectral range.

The energy of the most intense f−f band in these spectral data, at ~6200 cm^{-1}, exhibits an interesting and highly conserved trend: $E_{(F^-)}$ = 6172 (**3**), 6142 (**7**) < $E_{(Cl^-)}$ = 6241 (**4**), 6178 (**8**) < $E_{(Br^-)}$ = 6253 (**5**), 6190 (**9**) < $E_{(I^-)}$ = 6257 (**6**), 6198 (**10**) (all energies in cm^{-1}). It is also clear qualitatively that the splitting between the two excited-state energy levels that give rise to the two electronic transitions seen in these data is significantly larger for the fluoride complexes than for the other halide complexes for both imido ligand systems. The relationship describing the energy separation between these excited states and the ground state is a complicated function of both the spin–orbit coupling strength and the crystal field strength,[60,64] and on the basis of measurements of spacing between only these three levels (ground-state plus two excited-state levels), it is not possible to determine experimental values for the spin–orbit coupling parameter and the crystal-field splitting parameters. Further efforts to extract these parameters using a combination of theoretical calculations and experimental data are underway.

The final important observation from these electronic spectral data concerns the intensities in these f−f bands. The few reports of molar extinction coefficients for pentavalent uranium complexes pertain to complexes having octahedral or pseudo-octahedral symmetry, for which electric dipole transitions are forbidden to a first approximation and transitions gain intensity through vibronic mechanisms involving non-totally symmetric modes. Thus, for example, the more intense band normally assigned as a component in the $\Gamma_7 \rightarrow \Gamma_{7'}$ electronic transition at ~7000 cm^{-1} has an extinction coefficient, ϵ (in M^{-1} cm^{-1}), of ~5 for UF_6^-, ~14 for UCl_6^-, and ~22 for UBr_6^-.[15] In stark contrast, for **3**−**10**, the molar extinction coefficients are in the range from ~100 to 400 M^{-1} cm^{-1} for the more intense bands. As noted previously, the lower symmetry of these complexes leads to a relaxation of the electric-dipole selection rules, and this certainly contributes to the dramatic increase in the observed intensities here. However, it is likely that these f−f bands are also gaining some intensity from coupling to the nearby $\pi_{M=N} \rightarrow nb_{5f}$ charge-transfer transitions. A similar intensity-stealing mechanism has been observed for U^{IV}−ketimide complexes,[9,20] and the origin is similar in both the ketimide and imido series of complexes. Namely, there are metal f-orbitals that are common to both transitions that facilitate the mixing of charge-transfer character into the f−f transitions.

Magnetic Susceptibility. The paucity of organometallic U^V complexes has similarly resulted in few reports on their temperature-dependent magnetic behavior. The $5f^1$ electronic configuration for U^V results in a nominal electronic ground term of $^2F_{5/2}$ from $S = {}^1/_2$, $L = 3$, and $J = {}^5/_2$, and the predicted χT value for the U^V ion follows as 0.80 emu K mol^{-1} (2.54 μ_B) from the Russell–Saunders coupling scheme. As discussed above, ligand-field (LF) splitting of the $^2F_{5/2}$ term in a low-symmetry environment results in three Kramers doublets, with the ground term having a net magnetic moment. Reduction of the χT product with decreasing temperature results from thermal depopulation of these LF states. Figure 9 shows magnetic susceptibility data for complexes **6** and **10**, which are representative for **3**–**6** and **7**–**10**, and Table 8 lists the observed magnetic moments for the set of complexes obtained from linear fits of the high-temperature susceptibility data. These values are lower than the expected value but are consistent with those reported for U^V complexes.[13,14d,17,66–69]

(66) Edelstein, N. M.; Lander, G. H. Magnetic Properites. In *The Chemistry of the Actinide and Transactinide Elements*, 3rd ed.; Morss, L. R., Edelstein, N. M., Fuger, J., Eds.; Springer: The Netherlands, 2006; Vol. 4, pp 2241–2247.
(67) Miyake, C.; Hirose, M.; Ohya-Nishiguchi, H. *Inorg. Chim. Acta* **1989**, *165*, 179–183.
(68) Selbin, J.; Ahmad, N.; Pribble, M. J. *J. Chem. Soc., Chem. Commun.* **1969**, 759–760.
(69) Selbin, J.; Ahmad, N.; Pribble, M. J. *J. Inorg. Nucl. Chem.* **1970**, *32*, 3249–3258.

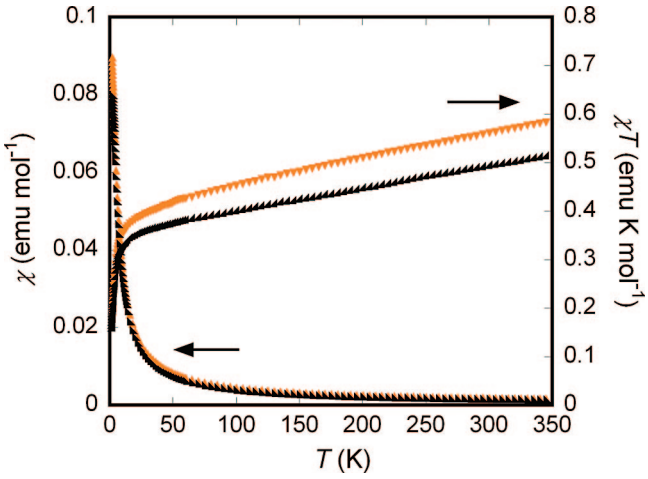

Figure 9. Magnetic susceptibilities and χT products of $(C_5Me_5)_2U(=N\text{-}2,4,6\text{-}{}^tBu_3\text{-}C_6H_2)(I)$ (**6**, orange) and $(C_5Me_5)_2U(=N\text{-}2,6\text{-}{}^iPr_2\text{-}C_6H_3)(I)$ (**10**, black) from 2 to 350 K.

Table 8. Magnetic Susceptibility Data for $(C_5Me_5)_2U(=N\text{-}Ar)(X)$ Complexes **3**–**10**

	Ar = 2,4,6-^{t}Bu$_3$-C$_6$H$_2$			Ar = 2,4,6-^{i}Pr$_2$-C$_6$H$_2$	
	X	μ_{eff} (μ_B/U)		X	μ_{eff} (μ_B/U)
3	F	2.46	**7**	F	2.22
4	Cl	2.51	**8**	Cl	2.42
5	Br	2.30	**9**	Br	2.42
6	I	2.53	**10**	I	2.34

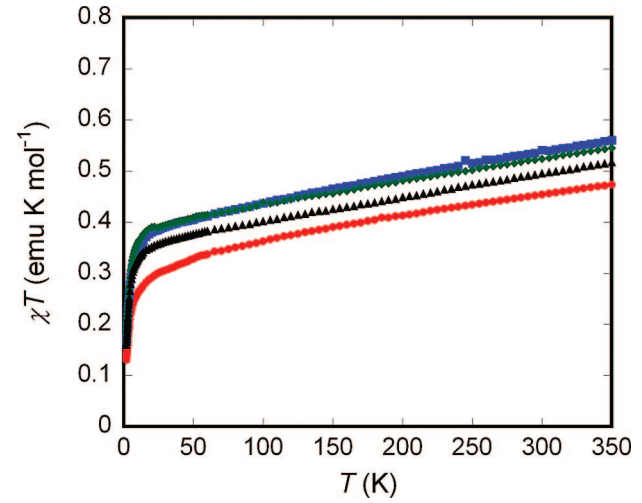

Figure 10. Temperature-dependent χT data for $(C_5Me_5)_2U(=N\text{-}2,6\text{-}{}^iPr_2\text{-}C_6H_3)(X)$ (**7**–**10**) from 2 to 350 K. Red, **7** (X = F); blue, **8** (X = Cl); green, **9** (X = Br); black, **10** (X = I).

The temperature dependence of the χT products for **7**–**10** is shown in Figure 10.[70] The data are generally similar in appearance, indicating no major changes in magnetic behavior based on the identity of the halide ion in these complexes. Their temperature dependences can be analyzed in terms of two general regimes of behavior: the high-temperature regime, from ~40 to 300 K, which is linear with large slopes, and the low-temperature regime, <40 K, where the χT products decrease precipitously. There are several instructive points to take from the appearance of these two regimes. In the high-temperature regime, all the LF states of the $^2F_{5/2}$ term are populated, such that the χT product is expected to reach the predicted value of 0.80 emu K mol^{-1}—though it clearly falls short in all the complexes here. The slopes of the linear regimes are due to the presence of temperature-independent paramagnetic (TIP) components from admixture of paramagnetic excited states into the ground state. The precipitous decrease of the LT regime is due to lifting of the $^2F_{5/2}$ term into its three ligand-field Kramers doublets and quenching of orbital angular momentum. On the basis of the magnetic data, it can be concluded that the total LF splitting energies are on the order of ~40 K in these complexes—consistent with data reported for other U^V−imido complexes.[66] This energetic splitting is significantly smaller than the result obtained from the simple spin–orbit LF calculation described above, which would appear to overestimate the splittings between the three doublets arising from the $^2F_{5/2}$ term. In future studies, we shall report additional spectroscopic and magnetic studies along with more sophisticated theoretical models to obtain a more detailed picture of the lowest energy levels of these U^V complexes.

In the context of the small amount of literature available, previous reports of U^V paramagnetism have asserted that the generally low magnetic moments for U^V complexes (compared to the L-S predicted value of 2.54 μ_B) arise from covalent character of the metal–ligand interaction that presumably results from siphoning of spin density from the metal to the ligand with an associated reduction in the orbital magnetism.[17,66] This would result in large differences in the room temperature magnetic moment for the complexes, dependent on geometry and the extent of metal–ligand overlap. However, negative correlation exists between complexes expected to show such a reduction due to large covalent metal–ligand interactions (**4**, μ_{eff} = 2.51 μ_B) and those whose interactions are primarily through σ donation (UCl_5, μ_{eff} = 1.42 μ_B).[13] Accompanying large differences in temperature-dependent susceptibilities, i.e., sensitivity of LF state energies to the ligands, are also not evident.[66] As such, it appears that simple conclusions on the extent of covalency as determined by room temperature magnetic moments for U^V complexes are not possible.

Conclusions

The series of U^V−imido halide complexes reported here have provided a valuable entry into the synthesis and characterization of pentavalent uranium organometallic complexes. The protocol is applicable to the full suite of halides, allowing for the synthesis of $(C_5Me_5)_2U(=N\text{-}Ar)(X)$ (where Ar = 2,6-^{i}Pr$_2$-C$_6$H$_3$ or 2,4,6-^{t}Bu$_3$-C$_6$H$_2$, and X = F, Cl, Br, I) from the corresponding U^{IV}−imido precursors, $(C_5Me_5)_2U(=N\text{-}Ar)$. Structural analyses, electrochemical and spectroscopic studies, and DFT calculations provide a coherent description of the electronic structure of these systems and indicate that both the U−X and U=N bonds exhibit covalency. The qualitative picture of the energy levels that emerges from both absorption spectra and the calculations shows that the f−f excitations occur at low energies and both charge-transfer and ligand-based excitations arise at higher energies, where the latter transitions involve excitations from M=N bonding orbitals to either 5f orbitals or ligand-based π^* orbitals. The electrochemical analysis shows that the ligand framework can stabilize both the U^{IV} and U^{VI} oxidation states, and the DFT results provide insights into the charge redistribution and structural changes occurring in these redox processes. While the halide series is not broad enough to allow us to make generalizations, studies involving the reactivity of these

(70) For a plot of the temperature dependence of the susceptibilities for **3**−**6**, see the Supporting Information.

U^V−imido halides for the synthesis of non-halogenated U^V−imido complexes $(C_5Me_5)_2U(=N\text{-}Ar)(L)$ (L ≠ F, Cl, Br, I) are currently underway. It is anticipated that expansion of this series to include non-halogenated derivatives will provide greater insight into the electronic structure of these pentavalent uranium systems and allow for the development of a comprehensive theoretical model that is consistent with the data obtained from electrochemical, spectroscopic, and magnetic measurements.

When considered in the broader context of other recent results for organouranium complexes, the results presented here for the U^V−imido complexes provide an important bridge between the data for U^{VI}−imido systems (e.g., $(C_5Me_5)_2U(=N\text{-}Ar)_2$), which have long been regarded as possessing substantial covalency in the metal–ligand multiple bonds, and the more recent data for U^{IV}−ketimide systems (e.g., $(C_5Me_5)_2U(-N=C\text{-}Ar_2)_2$), which possess metal–ligand bonding intermediate between single and double bonds on the basis of structural data. All three systems, $(C_5Me_5)_2U(=N\text{-}Ar)_2$, $(C_5Me_5)_2U(=N\text{-}Ar)(X)$, and $(C_5Me_5)_2U(-N=C\text{-}Ar_2)_2$, exhibit similar experimental hallmarks for covalent metal–ligand bonding. While it is not possible to make quantitative comparisons regarding the degree of covalency from the existing data, the emerging picture is that all three uranium oxidation states are able to support covalent bonding in these organometallic complexes.

Experimental Section

Instrumentation and Sample Protocols. Electronic absorption spectral data were obtained for toluene or toluene-d_8 solutions of complexes over the wavelength range 300–2500 nm on a Perkin-Elmer model Lambda 950 UV–visible−NIR spectrophotometer. Data were collected in 1 cm and 1 mm path length cuvettes loaded in a recirculating Vacuum Atmospheres NEXUS model inert atmosphere (N_2) drybox equipped with a 40CFM Dual Purifier NI-Train and run versus the appropriate toluene solvent reference. Samples were typically run at multiple dilutions to optimize absorbance in the UV–visible and near-infrared regions, respectively. Spectral resolution was typically 2 nm in the visible region and 4–6 nm in the near-infrared.

Voltammetric data were obtained in the Vacuum Atmospheres drybox system described above. In addition, data for complex **7** were obtained in a Schlenk-line electrochemical cell immersed in a dry ice/2-propanol bath at ∼−50 °C. All data were collected using a Perkin-Elmer Princeton Applied Research Corp. (PARC) model 263 potentiostat under computer control with PARC model 270 software. All sample solutions were ∼1–2 mM in complex with 0.1 M $[Bu_4N][B(3,5\text{-}(CF_3)_2\text{-}C_6H_3)_4]$ or $[Bu_4N][B(C_6F_5)_4]$ supporting electrolyte in THF solvent. All data were collected with the positive-feedback IR compensation feature of the software/potentiostat activated to ensure minimal contribution to the voltammetric waves from uncompensated solution resistance (typically ∼1 kΩ under the conditions employed). For experiments at ambient temperature, solutions were contained in PARC model K0264 microcells consisting of a ∼3 mm diameter Pt disk working electrode, a Pt wire counter electrode, and a Ag wire quasi-reference electrode. For the low-temperature experiment, a Schlenk cell was employed consisting of Pt wire working and counter electrodes sandwiching a Ag wire quasi-reference electrode. Scan rates from 20 to 5000 mV/s were employed in the cyclic voltammetry scans to assess the chemical and electrochemical reversibility of the observed redox transformations. Half-wave potentials were determined from the peak values in the square-wave voltammograms or from the average of the cathodic and anodic peak potentials in the reversible cyclic voltammograms. Potential calibrations were performed at the end of each data collection cycle using the ferrocenium/ferrocene couple as an internal standard. Electronic absorption and cyclic voltammetric data were analyzed using Wavemetrics IGOR Pro (version 4.0) software on a Macintosh platform.

Magnetic susceptibility data were collected using a Quantum Design Superconducting Quantum Interference Device (SQUID) magnetometer at 5 T from 2 to 350 K. The samples were sealed in a 5 mm Wilmad 505-PS NMR tube along with a small amount of quartz wool, which held the sample near the tube center. Contributions to the magnetization from quartz wool and the NMR tube were measured independently and subtracted from the total measured signal. Diamagnetic corrections were made with the use of Pascal's constants.

For the X-ray absorption measurement, $(C_5Me_5)_2U(=N\text{-}2,4,6\text{-}{}^tBu_3\text{-}C_6H_2)(Cl)$ (**4**) was loaded under a helium atmosphere into two nested aluminum sample holders equipped with Kapton windows. One set of windows was glued on, and one set was sealed with indium wire. The sample holder was shipped under He in a sealed container that was opened at the beam-line, immediately attached to the coldfinger of a liquid N_2 cryostat, and quickly evacuated (10^{-5} Torr). The cryostat was cooled with liquid N_2, and the X-ray absorption fine structure (EXAFS) spectrum was measured at the Stanford Synchrotron Radiation Laboratory, under dedicated operating conditions (3.0 GeV, 5%, 100 mA) on end station 10-2. A single energy was selected from the white beam with a liquid-N_2-cooled double-crystal monochromator utilizing Si[220] crystals. The crystals were run fully tuned, and a flat Pt-coated mirror, tilted to have a cutoff energy of 20–22 keV, was used to eliminate harmonics. The energy of the first inflection point of an Y foil, whose spectrum was measured within the same scan as the sample using the transmitted portion of the beam, was defined as 17032.08 eV. The spectra were measured in the fluorescence mode using a 30-element Ge detector and digital amplifiers. The signals from the different detector channels were examined individually and averaged by weighting them to maintain a constant signal:noise ratio. Dead times were set at ∼1.2 μs.

Using an in-house program, the averaged spectrum of **4** was normalized to a per-atom basis by offsetting the spectrum so that the value of a polynomial fit through the pre-edge region equaled zero at 17185 eV and then scaled so that the value of a polynomial fit through the post-edge region equaled unity at this same energy. The EXAFS were extracted from the spectrum by initially subtracting out the absorption edge and part of the white line determined by curve-fitting the edge region with the sum of an arctangent and asymmetric Gaussian fit to the absorption edge and peak. The smooth atomic-like background, which was approximated with a spline polynomial whose knots were set to minimize the area of the Fourier transform modulus of the spectrum over the region R = 1–1.1 Å, was then subtracted. Finally, the data were divided by the absorption falloff calculated from the McMaster tables.[71,72] The Fourier transform metrical parameters were extracted from the EXAFS by nonlinear least-squares curve-fitting of the χ data using amplitudes and phases calculated by FEFF7.[51] The ionization energy was constrained to be the same for each shell of the fit. Errors were calculated by determining the contribution of each shell to the overall error of the fit and then finding the shift in this parameter that resulted in the error being higher by 10% of this contribution.

Synthesis. The synthesis of complexes **3**–**5** and **7**–**9** is similar to that previously reported for the preparation of **6** and **10**.[23] A generic procedure is reported here for complexes **3**–**5** and **7**–**9**: To a stirring solution of **1** or **2** (0.50 g, 0.65 mmol) in toluene (50 mL) was added CuX_n (3.25 mmol; X = F, n = 2; X = Cl or Br,

(71) McMaster, W. H.; Del Grande, N. K.; Mallett, J. H.; Hubbel, J. H. *Lawrence Livermore National Laboratory Report UCRL-t0174, Section II Revision 1*; Lawrence Livermore National Laboratory: Livermore, CA, 1969; p 70.

(72) Hubbell, J. H.; McMaster, W. H.; Del Grande, N. K.; Mallett, J. H. In *International Tables for X-Ray Crystallography*; Ibers, J. A., Hamilton, W. C., Eds.; Kynoch Press: Birmingham, 1974; Vol. 4, pp 47–70.

$n = 1$) as a solid. The reaction vessel was sealed, and the solution was stirred at room temperature. After 12 h, the reaction was filtered through a Celite-packed coarse-porosity fritted filter, the filtrate was collected, and the volatiles were removed under reduced pressure. The resulting dark brown solid was taken up into hexanes and refiltered through a Celite-packed coarse-porosity fritted filter. Solvents were removed from the filtrate to give the product as a dark brown solid collected in isolated yields ranging from 75 to 89%. (See Supporting Information for additional details.)

Caution:*Depleted uranium (primary isotope ^{238}U) is a weak α-emitter (4.197 MeV) with a half-life of 4.47 × 10^9 years; manipulations and reactions should be carried out in monitored fume hoods or in an inert atmosphere drybox in a radiation laboratory equipped with α- and β-counting equipment.*

Computational Methods. The B3LYP hybrid density functional was employed to optimize the equilibrium molecular structures of the model complexes $(C_5Me_5)_2U(=N\text{-}C_6H_5)(F)$ (**11**) and $(C_5Me_5)_2U(=N\text{-}C_6H_5)(I)$ (**12**).[73] The calculations incorporate pentamethylcyclopentadienyl (C_5Me_5) ligands rather than adopting the computationally simpler strategy of using C_5H_5 as a C_5Me_5 surrogate. The substituted imido groups ($=N\text{-}2,4,6\text{-}{}^tBu_3\text{-}C_6H_2$) and ($=N\text{-}2,6\text{-}{}^iPr_2\text{-}C_6H_3$) were modeled as a phenyl group ($=N\text{-}C_6H_5$) for simplicity. The Stuttgart RSC 1997 effective core potential (ECP) was employed for uranium, which incorporates scalar relativistic effects and replaces 60 core electrons.[74] The valence electrons are represented as [6s/6p/5d/3f]; 6-31G* basis sets were used for carbon, hydrogen, and nitrogen. The fluorine and iodine atoms were represented by 6-311G* basis sets. For the iodide complex **12**, calculations using a relativistic ECP (RECP) for iodide using (Lanl2dz)[75] basis plus one polarization function were also compared with the all-electron calculations. The geometries from the all-electron and RECP calculation were very similar, with the main difference being that the U−I bond length was slightly shorter for the RECP model (0.02 Å) compared to the all-electron results. Bond angles differed by 2°, and very little difference was observed in the orbital composition or energies of the MOs. Unless otherwise specified, the results in the paper are reported from the all-electron calculations, which were all carried out using the Gaussian03 suite of codes.[76]

To estimate the effects of spin–orbit coupling on the 5f manifold, a simple ligand field model was employed. The calculated f energy levels and orbitals were obtained from a DFT calculation in which one electron was averaged over the 5f manifold. Using a one-center spin–orbit coupling operator with $\lambda_{SO} = 1800\ cm^{-1}$, the 14 × 14 spin–orbit matrix was diagonalized to obtain the seven Kramers doublet levels.

Acknowledgment. For financial support of this work, we acknowledge LANL (Director's PD Fellowship to C.R.G. and Frederick Reines PD Fellowship to E.J.S. and S.A.K.), the LANL G. T. Seaborg Institute (PD Fellowships to C.R.G. and P.Y.; summer graduate student fellowship to A.E.V.), the Division of Chemical Sciences, Office of Basic Energy Sciences, Heavy Element Chemistry program, and the LANL Laboratory Directed Research & Development program. The authors thank Kevin S. Boland, Carol J. Burns, Juan S. Lezama, Marianne P. Wilkerson, and Laura E. Wolfsberg (all LANL) for assistance with the EXAFS measurement on complex **4**.

Supporting Information Available: General experimental consideration; full characterization details for **3**−**5**, **7**−**9**; crystallographic data (CIF) for **2**, **3**, **5**, **8**, **9**; XYZ data for **11**, **12**; and complete ref 76. This material is available free of charge via the Internet at http://pubs.acs.org.

JA711010H

(73) Becke, A. D. *J. Chem. Phys.* **1993**, *98*, 5648–5652.
(74) Kuechle, W.; Dolg, M.; Stoll, H.; Preuss, H. *J. Chem. Phys.* **1994**, *100*, 7535–7542.
(75) Hay, P. J.; Wadt, W. R. *J. Chem. Phys.* **1985**, *82*, 270–283.
(76) Frisch, M. J.; et al. *Gaussian 03*; Gaussian, Inc.: Wallingford, CT, 2004.